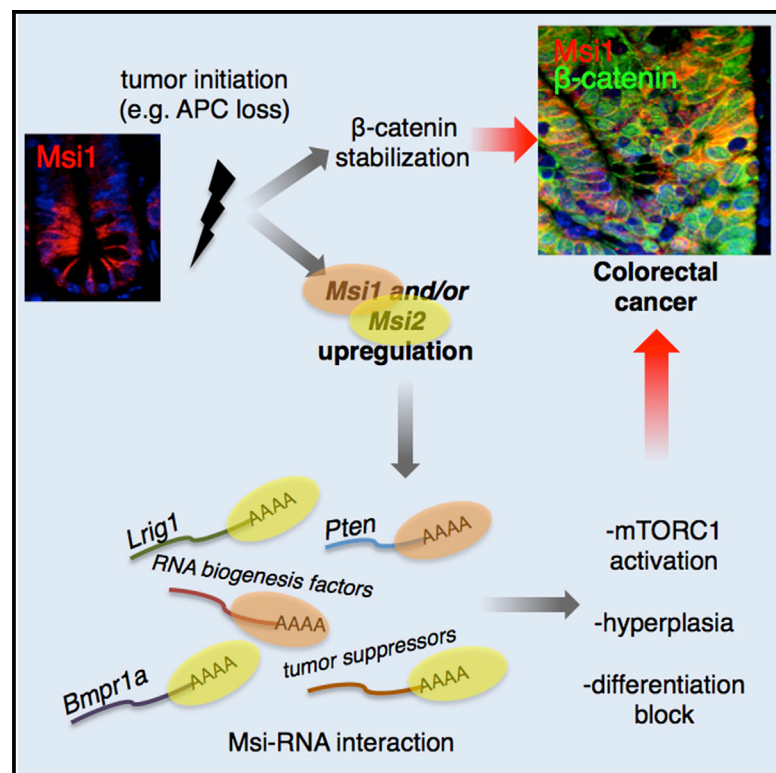


# Cell Reports

## The Msi Family of RNA-Binding Proteins Function Redundantly as Intestinal Oncoproteins

### Graphical Abstract



### Authors

Ning Li, Maryam Yousefi, Angela Nakauka-Ddamba, ..., Brian D. Gregory, Zhengquan Yu, Christopher J. Lengner

### Correspondence

zyu@cau.edu.cn (Z.Y.), lengner@vet.upenn.edu (C.J.L.)

### In Brief

Expression of the Msi family of RNA-binding proteins is observed in intestinal stem cells and colorectal cancers. Li et al. demonstrate that Msi1 and Msi2 are functionally redundant oncoproteins that are required for colorectal cancer initiation and maintenance in a pathway parallel to β-catenin, where they drive mTORC1 activation.

### Highlights

- RNA-binding proteins Msi1 and/or Msi2 are required for colorectal cancer
- Msi1/2 are functionally redundant with similar target transcripts
- Msi proteins function independently of β-catenin to promote tumorigenesis

### Accession Numbers

GSE74321  
GSE54598



# The Msi Family of RNA-Binding Proteins Function Redundantly as Intestinal Oncoproteins

Ning Li,<sup>1,13</sup> Maryam Yousefi,<sup>9,13</sup> Angela Nakauka-Ddamba,<sup>13</sup> Fan Li,<sup>5,8</sup> Lee Vandivier,<sup>5,9</sup> Kimberly Parada,<sup>13</sup> Dong-Hun Woo,<sup>13</sup> Shan Wang,<sup>1,13</sup> Ammar S. Naqvi,<sup>5</sup> Shilpa Rao,<sup>6</sup> John Tobias,<sup>6</sup> Ryan J. Cedeno,<sup>9,13</sup> Gerard Minuesa,<sup>3</sup> Katz Y,<sup>2</sup> Trevor S. Barlowe,<sup>3</sup> Alexander Valvezan,<sup>9,10</sup> Sheila Shankar,<sup>13</sup> Raquel P. Deering,<sup>2</sup> Peter S. Klein,<sup>9,10,12</sup> Shane T. Jensen,<sup>7</sup> Michael G. Kharas,<sup>3</sup> Brian D. Gregory,<sup>5,8</sup> Zhengquan Yu,<sup>1,\*</sup> and Christopher J. Lengner<sup>4,9,11,12,13,\*</sup>

<sup>1</sup>State Key Laboratories for Agrobiotechnology, College of Biological Sciences, China Agricultural University, Beijing 100194, China

<sup>2</sup>Broad Institute of Harvard and MIT, Cambridge, MA 02142, USA

<sup>3</sup>Molecular Pharmacology and Chemistry Program, Experimental Therapeutics Center and Center for Stem Cell Biology, Memorial Sloan-Kettering Cancer Center, New York, NY 10065, USA

<sup>4</sup>Center for Molecular Studies in Digestive and Liver Diseases

<sup>5</sup>Department of Biology, School of Arts and Sciences

<sup>6</sup>PENN Molecular Profiling Facility

<sup>7</sup>Department of Statistics, The Wharton School

<sup>8</sup>Genomics and Computational Biology Graduate Program

<sup>9</sup>Cell and Molecular Biology Graduate Program

<sup>10</sup>Department of Medicine, School of Medicine

<sup>11</sup>Department of Cell and Developmental Biology, School of Medicine

<sup>12</sup>Institute for Regenerative Medicine

<sup>13</sup>Department of Biomedical Sciences, School of Veterinary Medicine

University of Pennsylvania, Philadelphia, PA 19104, USA

\*Correspondence: [zyu@cau.edu.cn](mailto:zyu@cau.edu.cn) (Z.Y.), [lengner@vet.upenn.edu](mailto:lengner@vet.upenn.edu) (C.J.L.)

<http://dx.doi.org/10.1016/j.celrep.2015.11.022>

This is an open access article under the CC BY-NC-ND license (<http://creativecommons.org/licenses/by-nc-nd/4.0/>).

## SUMMARY

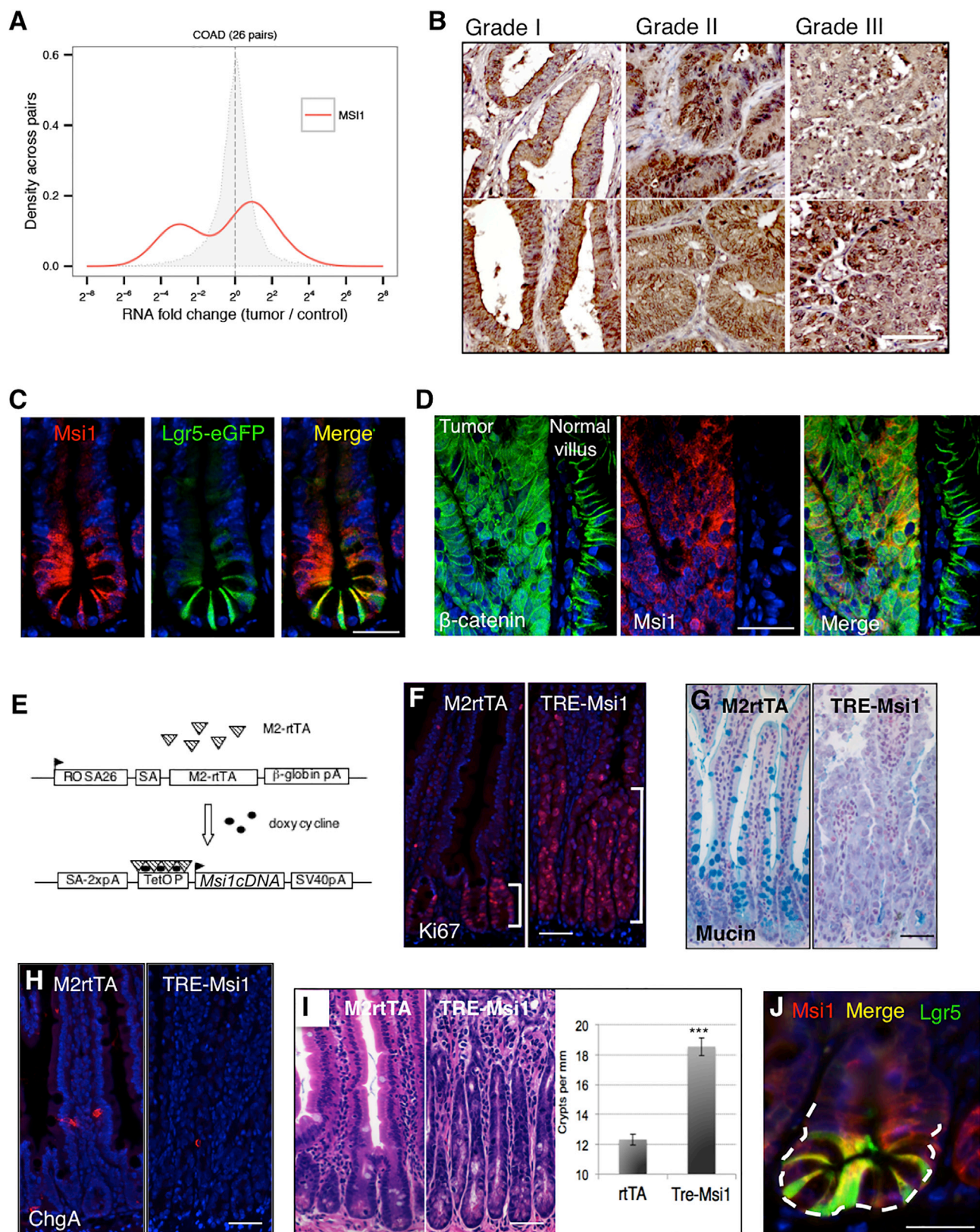
Members of the Msi family of RNA-binding proteins have recently emerged as potent oncoproteins in a range of malignancies. MSI2 is highly expressed in hematopoietic cancers, where it is required for disease maintenance. In contrast to the hematopoietic system, colorectal cancers can express both Msi family members, MSI1 and MSI2. Here, we demonstrate that, in the intestinal epithelium, Msi1 and Msi2 have analogous oncogenic effects. Further, comparison of Msi1/2-induced gene expression programs and transcriptome-wide analyses of Msi1/2-RNA-binding targets reveal significant functional overlap, including induction of the PDK-Akt-mTORC1 axis. Ultimately, we demonstrate that concomitant loss of function of both MSI family members is sufficient to abrogate the growth of human colorectal cancer cells, and *Msi* gene deletion inhibits tumorigenesis in several mouse models of intestinal cancer. Our findings demonstrate that MSI1 and MSI2 act as functionally redundant oncoproteins required for the ontogeny of intestinal cancers.

## INTRODUCTION

Mammalian orthologs of the *Drosophila melanogaster* Musashi RNA-binding protein include Msi1/MSI1 and Msi2/MSI2.

*Drosophila* Musashi governs asymmetric cell fate determination in neuroblasts through translational suppression of mRNAs encoding a lineage determinant (Nakamura et al., 1994; Okabe et al., 2001). A similar role for Msi2 in regulating asymmetric fate determination has been proposed based on analysis of asymmetric partitioning of the Msi RNA-binding target Numb in hematopoietic stem cells with Msi2 gain or loss of function (Kharas et al., 2010; Park et al., 2014). Besides a potential role in governing asymmetric cell division, Msi proteins act as potent oncoproteins in a number of cancers. In particular, Msi2/MSI2 is a cooperative oncoprotein in hematopoietic malignancies, where it sustains a cancer stem cell self-renewal program through interaction with a number of mRNA-binding targets (Ito et al., 2010; Kharas et al., 2010; Park et al., 2014, 2015). Whereas significant progress has been made in understanding the contribution of Msi2 to hematopoietic malignancies, very little is known about the functional contribution of Msi proteins to oncogenic transformation in other human malignancies and murine tumor models.

In the hematopoietic system, Msi2 is the only Msi family member expressed and its expression is largely restricted to the hematopoietic stem cell compartment. In contrast, Msi1 and Msi2 are coexpressed in the putative stem cell compartments of a variety of other tissues including the hair follicle (Sugiyama-Nakagiri et al., 2006), mammary gland (Clarke et al., 2003; Katz et al., 2014; Wang et al., 2008), germ cells (Sutherland et al., 2014), intestinal epithelium (Kayahara et al., 2003; Li et al., 2014; Potten et al., 2003; Wang et al., 2015), and neural epithelium (Sakakibara et al., 2002). The observation that both Msi1 and Msi2 are coexpressed in these tissues, coupled with an absence of phenotype upon genetic ablation of either *Msi1* or



(legend on next page)



*Msi2* (with the exception of compromised brain ventricle formation in *Msi1*<sup>-/-</sup> mice), and sequence homology between *Msi1* and *Msi2* strongly suggests that functional redundancy exists between *Msi* family members. This notion is supported by findings where knockdown of *Msi2* in ex vivo cultures of *Msi1*-null neurospheres inhibits self-renewal (Sakakibara et al., 2002).

Here, we compare the similarities between the oncogenic properties of *Msi1* and *Msi2* in the intestinal epithelium. Published studies have observed *Msi1* expression in both stem cells of the intestinal crypts and human colorectal cancers (CRCs), and several studies suggest that *Msi1* has mitogenic activity driven by potentiation of the canonical Wnt- and/or Notch-signaling pathways (Cambuli et al., 2015; Rezza et al., 2010; Spears and Neufeld, 2011; Sureban et al., 2008). Like *Msi1*, *Msi2* is also expressed in the stem cell compartment of intestinal crypts and is broadly overexpressed in CRC, and *MSI2* inhibition in SW48 and HT29 CRC cell lines has antiproliferative effects both in vitro and in murine xenografts (Wang et al., 2015). These findings suggest that *Msi1* and *Msi2* may have overlapping roles in promoting transformation of the intestinal epithelium; however, in vivo gain-of-function studies demonstrated that *Msi2*, unlike *Msi1*, does not potentiate canonical Wnt signaling and has little to no effect on activity of the Notch pathway as was reported for *MSI1* in CRC cell lines (Wang et al., 2015). Thus, there is uncertainty as to whether *Msi1* has oncogenic functions in the intestinal epithelium in vivo and whether *Msi1* and *Msi2* might function redundantly in promoting intestinal transformation.

Here, we demonstrate that acute, in vivo *Msi1* gain of function phenocopies that of *Msi2*, including expansion of intestinal crypt base columnar stem cells, blocked differentiation, upregulation of an APC-loss gene expression signature, and activation of the mTORC1 complex, all in a Wnt-independent manner. Comparison of transcriptome profiles derived from either *Msi1* or *Msi2* gain of function indicates that these family members are capable of activating similar gene expression programs, and comparison of transcriptome-wide, in vivo, *Msi1*- and *Msi2*-RNA-binding analyses reveals a similar repertoire of binding targets that function in analogous pathways. Ultimately, *Msi1/2* loss-of-function experiments demonstrate that the activity of

these RNA-binding proteins is required for the initiation and maintenance of intestinal cancers.

## RESULTS

### *Msi1* Is Expressed in Intestinal Cancers, and Its Forced Expression Transforms the Intestinal Epithelium

Several studies suggest that *MSI1* and *MSI2* are broadly expressed in CRCs (Levin et al., 2010; Li et al., 2011; Wang et al., 2015), although correlation of *MSI* expression with stage or grade is less clear. We sought to confirm *MSI1* expression in gastrointestinal cancers and observed both over- and underexpression relative to controls in a number of these malignancies (Figures 1A, 1B, S1A, and S1B). Interestingly, matched pairs of colorectal adenocarcinomas and normal adjacent tissue revealed *MSI1* expression to be more variable than that of *MSI2*, with *MSI1* overexpression observed in around half of these malignancies in comparison to the ubiquitous overexpression of *MSI2* (Figure 1A; Wang et al., 2015). We confirmed prior reports of *Msi1* expression in murine crypt base columnar intestinal stem cells (CBCs) and its upregulation in early adenomas resulting from loss of heterozygosity of the *APC* tumor suppressor in the *APC*<sup>min/+</sup> mouse model (Potten et al., 2003; Figures 1C and 1D). Given that *MSI2* is broadly expressed in CRC and is also upregulated upon *APC* loss, we generated a targeted, single-copy, doxycycline-inducible *Msi1* gain-of-function mouse model (*TRE-Msi1*) using genetic loci identical to those used to assess the consequences of *Msi2* gain of function (Wang et al., 2015). This enables direct comparison between the consequences of *Msi1* and *Msi2* activation (Figures 1E, S1C, and S1D). Doxycycline (Dox) administration resulted in broad induction of *Msi1* throughout the intestinal epithelium, but not in the underlying stromal mesenchyme or lacteals (Figure S1E). Control mice (*R26-M2rtTA* + Dox) exhibited no differences in *Msi1* expression patterns relative to wild-type (Figure S1E).

*Msi1* induction resulted in an expansion of the crypt proliferative zone and decreased presence of differentiated cells (the exception being persistence of Paneth cells, possibly due to their long lifespan and stable positioning at the crypt base; Figures

### Figure 1. *MSI1* Is Expressed in Colorectal Cancers and Is Sufficient to Transform the Epithelium

- (A) *MSI1* expression in matched tumor/control sample pairs from TCGA colorectal adenocarcinoma (COAD) RNA-seq (total of 26 patients). The distribution of *MSI1* fold changes in tumor/control pairs for 26 individuals is plotted in red (intra-individual comparison). The distribution of *MSI1* fold changes between control/control comparisons for 26 pairs of healthy individuals is plotted in gray (inter-individual comparison).
- (B) Immunohistochemical staining for *MSI1* in graded human colorectal cancer sections (scale = 100  $\mu$ m).
- (C) Immunofluorescence staining of *Msi1* (red) in stem cells of the intestinal crypt costained for the crypt base columnar stem cell marker *Lgr5* in *Lgr5-eGFP-IRES-CreER* knockin mice (green; scale = 50  $\mu$ m).
- (D) Immunofluorescence for  $\beta$ -catenin and *Msi1* in an adenoma resulting from *APC* LOH in the *APC*<sup>min/+</sup> mouse and normal villi adjacent to the adenoma (scale = 100  $\mu$ m).
- (E) Design of doxycycline (Dox)-inducible *Msi1* knockin mice harboring a modified reverse tetracycline transactivator (*M2rtTA*) at the *ROSA26* locus and the *Msi1* cDNA under control of the tetracycline-responsive element-minimal CMV promoter (*TRE/TetOP*) targeted to safe-haven chromatin downstream of the *Col1a1* locus.
- (F) Immunofluorescence staining for Ki-67 marking proliferative cells in the intestinal crypts of control (*M2rtTA*) and *TRE-Msi1* mice 48 hr after Dox induction.
- (G) Alcian blue staining for goblet cell mucin.
- (H) Immunofluorescence staining for the enteroendocrine marker chromogranin A (scale in F–H = 100  $\mu$ m).
- (I) Histological sections showing extension of crypt height and increased crypt fission in *TRE-Msi1* mice (quantified at right; n = 3 mice; \*\*\*p < 0.0005; Student's t test).
- (J) A crypt undergoing fission in *Lgr5-eGFP-IRES-CreER* knockin mice costained for *Msi1* (red) and GFP (green; scale = 50  $\mu$ m).
- See also Figure S1.



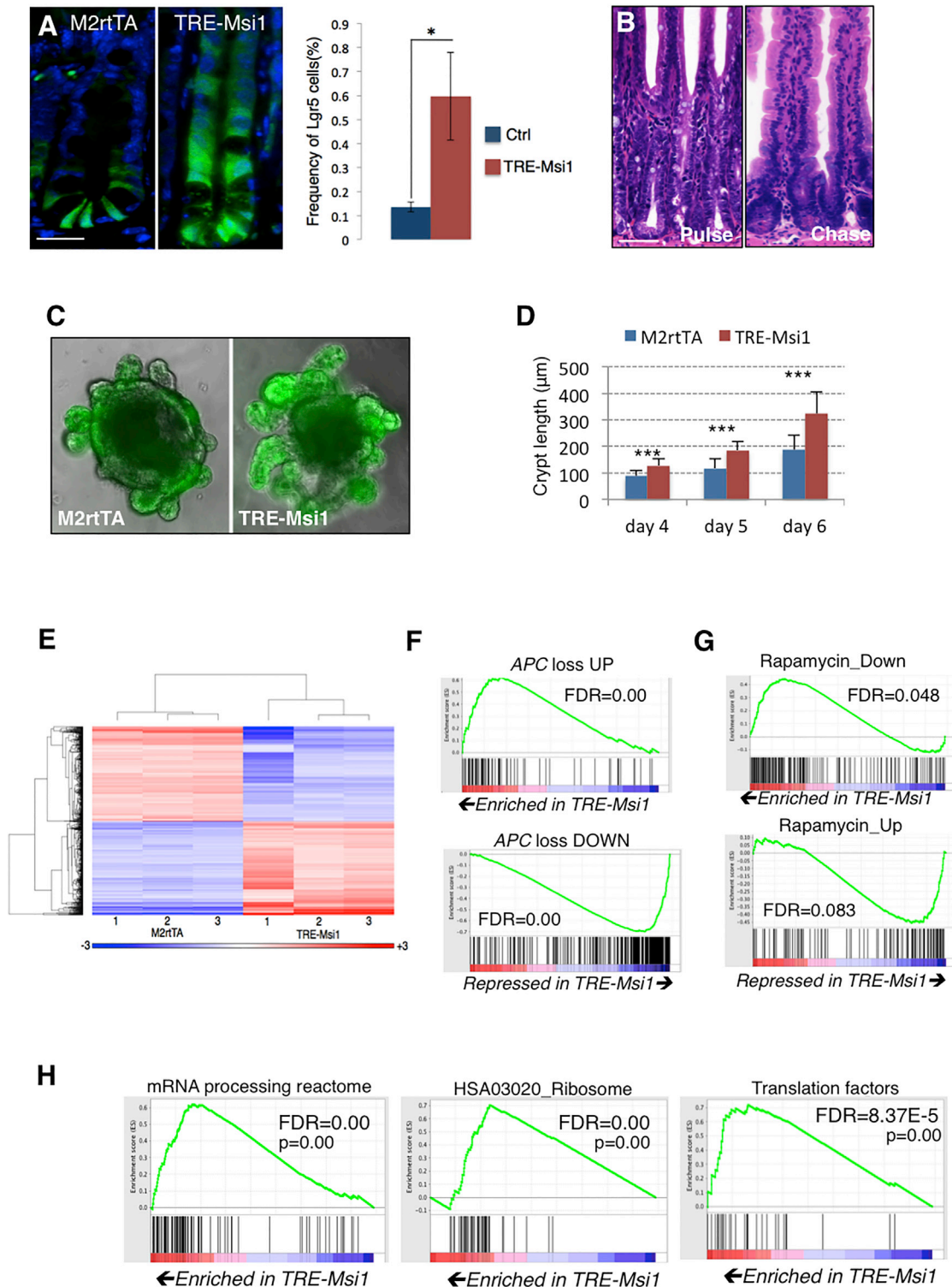


**Figure 2. Msi1 Induction Expands the Progenitor Cell Compartment and Drives APC Loss and RNA Metabolism Gene Expression Programs**  
(A) Msi1 induction in *TRE-Msi1::Lgr5-eGFP-CreER* mice results in an upward expansion of Lgr5-eGFP<sup>+</sup> cells and an increase in the absolute frequency of Lgr5-eGFP<sup>+</sup> cells, quantified by flow cytometry (right; n = 3 mice per group; \*p < 0.05; Student's t test; scale = 50  $\mu\text{m}$ ).  
(B) *TRE-Msi1* epithelium transformed by Dox induction for 48 hr revert to a phenotypically normal state persisting 2 months after Dox withdrawal (scale = 100  $\mu\text{m}$ ).  
(C and D) In vitro culture of intestinal organoids derived from *TRE-Msi1::Lgr5-eGFP-CreER* crypts followed by Dox induction in vitro. Crypt bud length is quantified in (D) (\*\*p < 0.0005; Student's t test).

(legend continued on next page)

1F–1H and S1F–S1I). This caused *TRE-Msi1* mice to become dehydrated, requiring euthanasia after approximately 3 days of Dox exposure. Msi1 induction also increased crypt fission, and endogenous Msi1 colocalized with Lgr5+ CBCs at sites of crypt fission in wild-type mice (Figures 1I and 1J). We next examined the effects of Msi1 induction on CBCs in *TRE-Msi1::Lgr5-eGFP-CreER* mice and observed an upward expansion of the stem cell zone and a significant increase in the frequency of Lgr5-eGFP+ CBCs (Barker et al., 2007; Figure 2A). Dox withdrawal resulted in a reversion of the epithelium to the wild-type state, which was maintained for several months, indicating that, upon Msi1 downregulation, crypt stem cells return to a niche-dependent homeostatic state (Figure 2B). Further, Msi1 induction in ex vivo cultures of Lgr5-eGFP+ crypts resulted in increased growth of crypt buds, indicating that the phenotype is epithelial cell-autonomous (Figures 2C and 2D).

All of the phenotypes resulting from Msi1 induction are consistent with those observed in response to Msi2 induction and are also consistent with acute loss of APC (excepting the stable positioning of Paneth cells, which become mislocalized upon APC loss; Sansom et al., 2004; Wasan et al., 1998). Thus, Msi1 induction in vivo phenocopies that of Msi2 in otherwise genetically identical mouse models.

### Msi1 and Msi2 Drive Common Gene Expression Programs and Interact with Common Target Transcripts

We next analyzed changes to the transcriptome resulting from Msi1 induction (Table S1). Consistent with our phenotypic observations, unbiased gene set enrichment analysis (GSEA) (Subramanian et al., 2005) demonstrates that the APC-loss gene signature is among the most highly enriched upon Msi1 induction (Figures 2E and 2F; Table S2). We also observed enrichment of gene sets related to mRNA processing and translation along with an inverse correlation between the Msi1-induced gene expression program and expression profiles induced by the mTORC1 inhibitor rapamycin (Figures 2G and 2H). All of these gene signatures were similarly enriched in intestinal epithelium overexpressing Msi2 (Wang et al., 2015), indicating that the analogous phenotypes resulting from Msi1 or Msi2 induction are driven by analogous gene expression programs. We therefore directly compared Msi1- and Msi2-induced transcriptome profiles and observed that 72% of gene expression changes resulting from Msi1 induction also occurred upon Msi2 induction (Figure 3A). Gene ontology (GO) and pathway analysis found commonly upregulated programs involved in ribosome biogenesis, signal transduction, and ErbB signaling, among others (Table S3). Commonly downregulated programs were broadly related to oxidative phosphorylation and mitochondrial activity.

Given that Msi1/2 are RNA-binding proteins that act on translation (Battelli et al., 2006; Katz et al., 2014; Kawahara et al.,

2008; Okano et al., 2002), we performed in vivo transcriptome-wide RNA-binding analysis (CLIP-seq) for both endogenous and induced Msi1 in the intestinal epithelium to identify direct targets. Msi1 bound 2,371 transcripts in wild-type crypts, primarily in 3' UTRs and coding sequences (Figure 3B; Table S4). Upon Dox administration, ectopic Msi1 became increasingly associated with intronic sequences, and 91% of transcripts newly bound upon Msi1 induction (i.e., those transcripts associated only with ectopic Msi1) were bound in introns (Figures 3B and S2A). In total, 93% of transcripts bound by Msi1 in wild-type crypts were also bound in *TRE-Msi1* epithelium (Figure 3C). These binding patterns were consistent with those previously described for Msi2.

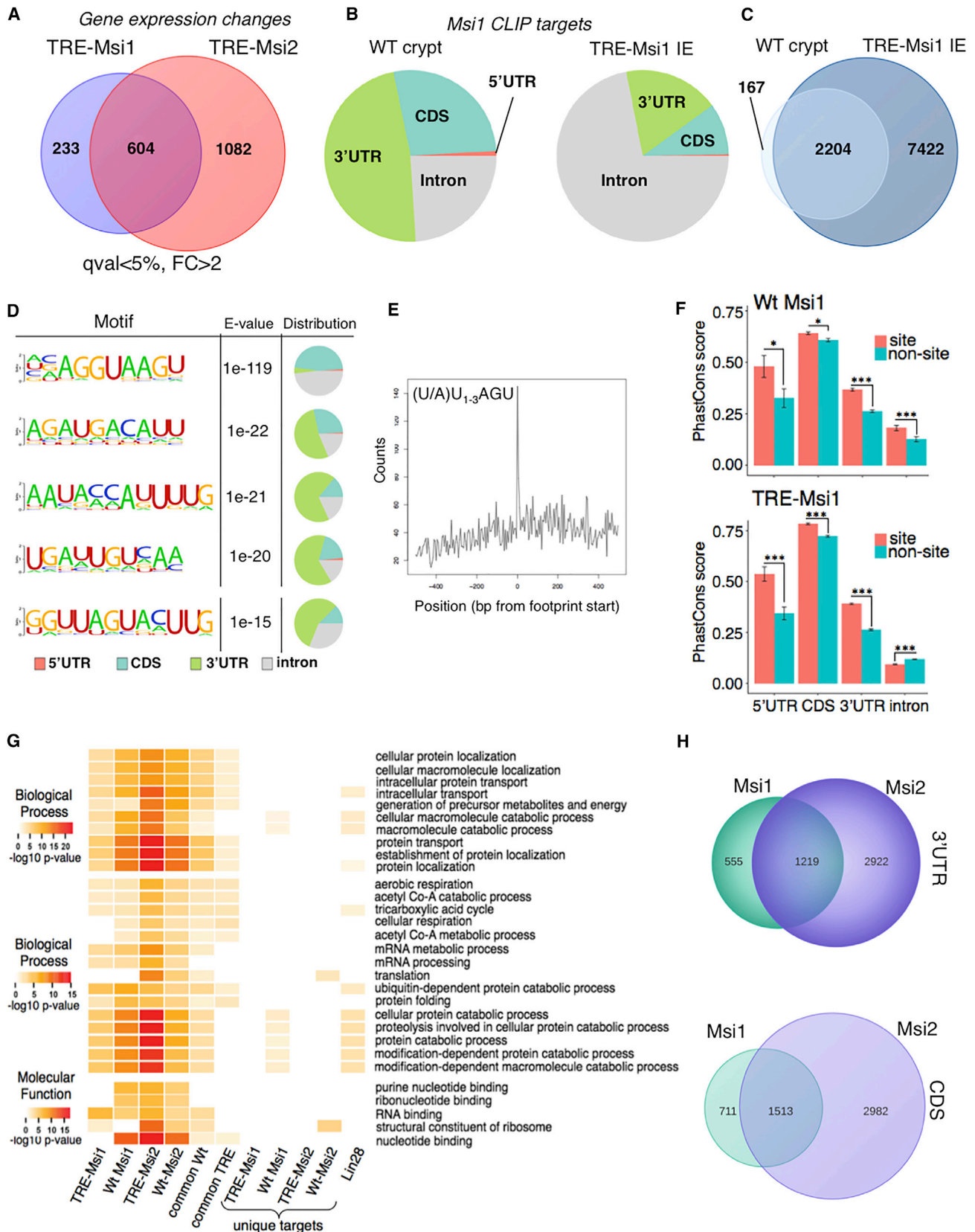
Motif analysis of CLIP targets indicated that Msi1 binds distinct sequences in introns and coding sequences in comparison to 3' UTRs, and although Msi1-binding motifs were A-U rich, the previously described Msi1 motif discovered by a SELEX-based approach ((A/U)U<sub>1-3</sub>AGU; Imai et al., 2001) was not among the most significant (Figure 3D). It was, however, significant in the data set and was located in the center of sequence reads containing it, demonstrating that it is a bona fide motif in vivo (Figures 3D and 3E). Msi1 binding showed no preference for highly abundant transcripts, and globally, transcripts newly bound upon Msi1 induction exhibited no change in their expression levels (Figures S2B and S2C). Sequence-specific Msi1-RNA interactions were confirmed using in vitro binding assays incubating recombinant human Msi1 with RNA oligos containing the consensus motifs identified by CLIP (Figure S2D).

The large number of intronic binding sites led us to further investigate Msi1-intronic interaction. Nuclear/cytoplasmic fractionation of wild-type crypts and human CRC cells indicates that the majority of Msi1 is cytoplasmic, and binding site conservation analysis demonstrates that, whereas all binding sites for endogenous Msi1 and the UTR and coding sequence sites for ectopic Msi1 are evolutionarily conserved, intronic binding sites of ectopic Msi1 are not (Figures 3F and S2E). These data suggest that intronic binding events for ectopic Msi1 may be largely promiscuous. Consistent with this, analysis of the location of Msi1-binding sites across introns revealed a preference for interaction of Msi1 with the 5' intron terminus in wild-type crypts, and this preference was largely attenuated for ectopic Msi1 (Figure S2F). This also suggests that some Msi1-intron interactions may be involved in alternative splicing (Katz et al., 2014; Uren et al., 2015). We therefore asked how Msi1 binding was related to exon inclusion/exclusion. Interestingly, Msi1 targets were more likely to contain exons that exhibited increased inclusion upon ectopic Msi1 induction than transcripts not bound by Msi1, further suggesting that Msi1 activity may be associated with alternative exon inclusion (Figure S3A).

(E) Heatmap and hierarchical clustering of transcriptome profiles performed on the intestinal epithelium of three control (*M2rtTA*) and three *TRE-Msi1* mice treated with Dox for 24 hr.

(F–H) Gene set enrichment analysis (GSEA) of the *TRE-Msi1* transcriptome identifies activation of genes induced by acute APC deletion in the intestinal epithelium (APC loss up) and suppression of genes downregulated after APC deletion (APC loss down; F), along with an anti-correlation between the Msi1-induced transcriptome profile and the Peng\_Rapamycin UP/DOWN gene sets (G) and an enrichment of expression of mRNA processing, ribosomal, and translation factors upon Msi1 induction (H). FDR, false discovery rate.

See also Tables S1 and S2.



(legend on next page)



GO analysis revealed that Msi1 binds transcripts encoding regulators of RNA metabolism, nucleotide binding, and cellular respiration consistent with the GSEA analysis of transcriptome changes (Figure 3G; Table S5). Significantly enriched GO categories also included protein localization and transport, possibly reflecting an established role for Msi in governing asymmetric cell fate determination (Kharas et al., 2010; Nakamura et al., 1994). These pathways were not enriched in the set of targets of an unrelated RNA-binding protein Lin28b (Madison et al., 2013). Consistent with the GSEA and GO analyses, Ingenuity Pathway Analysis identified pathways involved in cellular respiration, cancer, and Pten-PI3K-AKT-mTORC1 signaling as being the most significantly represented across the CLIP data sets (Figure S3B).

We next sought to determine the overlap in the RNA-binding activities of Msi1 and Msi2 and observed that 69% and 68% of transcripts bound by wild-type Msi1 in their 3' UTR and coding sequences, respectively, were similarly bound by Msi2 (Figure 3H). Similar binding patterns were observed for ectopically induced Msi1 and Msi2 (Figure S3C). Both Msi1 and Msi2 targets functioned in analogous pathways, including RNA metabolism, protein localization, and cellular respiration (Figures 3G and S3B; Tables S5 and S6). Further, overlap of our murine in vivo CLIP data sets with published RNA-binding data for MSI1 in human transformed cell lines in vitro (de Sousa Abreu et al., 2009; Uren et al., 2015; Vo et al., 2012) reveals a significant overlap despite the vast differences in cellular identity (Figure S4A). These analyses indicate that Msi1/MSI2 act on a common set of target genes, accounting for the identical phenotype between Msi1 and Msi2 gain of function. Given their highly similar RNA-binding activities, we tested for Msi1-Msi2 protein interaction but failed to detect any by co-immunoprecipitation, suggesting that either Msi1 or Msi2 are sufficient to act upon target transcripts (Figure S4B).

The transcripts encoding p21 and Numb are among the best-characterized Msi1 targets (Battelli et al., 2006; Imai et al., 2001), and we previously observed Msi2 binding to these transcripts in the intestinal epithelium (Wang et al., 2015). Similarly, these transcripts were bound by ectopically induced Msi1 (Figure S4C). Msi1 also bound the transcripts encoding the well-established intestinal tumor suppressors Lrig1 and Bmpr1 (He et al., 2004; Powell et al., 2012), as we previously observed for Msi2 (Figure 4A). Interestingly, Lrig1 is a negative regulator of ErbB signaling, and we observed upregulation of the ErbB pathway downstream of both Msi1 and Msi2 (Table S3).

### Msi1 Does Not Potentiate Transcriptional Activity of the Canonical Wnt Pathway

Msi1 has been reported to bind to and inhibit the function of APC, a negative regulator of the transcriptional effector or canonical Wnt signaling,  $\beta$ -catenin (Spears and Neufeld, 2011), and in vitro studies have posited a role for Msi1 in potentiating canonical Wnt target gene expression (Rezza et al., 2010). Indeed, we observed binding of the APC transcript; however, we also observed stronger binding of Msi1 to the *Ctnnb1* transcript encoding  $\beta$ -catenin (Figure 4A). We confirmed the preference of endogenous human MSI1 for CTNNB1 versus APC using CLIP-qRT-PCR, and this binding preference was maintained upon Wnt pathway stimulation with the GSK3 $\beta$ -inhibitor CHIR 99021 (Figure 4B). 3' UTR luciferase reporter assays confirmed that MSI1 repress CTNNB1 translation, albeit moderately (Figure 4C). Similarly, activity of the TOPFlash multimerized  $\beta$ -CATENIN/TCF reporter was attenuated by MSI1 activity (Figure 4D). To determine the effects of Msi1 activity on the canonical Wnt pathway in vivo, we examined APC and  $\beta$ -catenin protein in control and *TRE-Msi1* epithelium and observed no appreciable differences (Figures 4E–4G). Further, analysis of the expression of direct  $\beta$ -catenin target genes in *TRE-Msi1* epithelium showed no significant changes upon Msi1 induction (Figure 4H). Thus Msi1, like Msi2, does not potentiate canonical Wnt signaling in vivo.

### Msi1 Activates the PDK-Akt-mTORC1 Axis

One of the major oncogenic pathways downstream of Msi2 is mTORC1, which becomes activated upon Msi2 binding to its upstream inhibitor Pten (Wang et al., 2015). Msi1 also bound to the 3' UTR of the Pten mRNA, decreasing Pten protein levels (Figures 5A and 5B). Further, MSI knockdown in human CRC cells led to increased PTEN activity and decreased PIP3 levels (Figures 5C and S5A–S5C). Downstream of Pten, Msi1 induction activated the PDK-Akt-mTORC1 axis (Figures 5B and 5D), with increased phosphorylation of AKT at T308 by PDK1 (PDPK1). AKT phosphorylation at S473 by mTORC2, however, showed only a minor increase, indicating that mTORC1 activation is due to increased AKT activity via activation of AKT by the PI3K pathway. Consistent with this notion, we observed an increase in the activating PDK1 autophosphorylation event at S241 (Figure 5D) and increased phosphorylation of the AKT target c-RAF (S259), further supporting the activation of AKT downstream of Msi1. Downstream of mTORC1, there was strong inactivating phosphorylation of the translational inhibitor 4EBP1, resulting in

#### Figure 3. Msi1 and Msi2 Have Overlapping RNA-Binding Targets

(A) Venn diagram showing the degree of overlap in gene expression changes driven by Msi1 versus Msi2 induction in transcriptome profiles of the *TRE-Msi1* and *TRE-Msi2* intestinal epithelium.

(B) Distribution of Msi1-RNA binding events for endogenous Msi1 in wild-type crypts (left) and induced Msi1 in *TRE-Msi1* intestinal epithelium (right).

(C) Venn diagram showing the degree of overlap in Msi1 RNA-binding targets wild-type crypts and in *TRE-Msi1* intestinal epithelium.

(D) Msi1-binding motif identification and distribution in wild-type intestinal crypts. The fifth motif represents the motif previously identified by selex in vitro.

(E) Position of the canonical Msi1 recognition motif previously identified in vitro within CLIP-seq reads containing that motif.

(F) PhastCons analysis of conservation of Msi1-binding sites in the indicated regions of Msi1 target transcripts. Error bars represent 95% confidence intervals;

\*p < 0.05; \*\*p < 0.005; \*\*\*p < 0.0005.

(G) Gene ontology analyses for biological processes and molecular functions that are significantly enriched in Msi1/*TRE-Msi1* or Msi2/*TRE-Msi2* CLIP data sets, as well as for gene sets common to both wild-type or ectopic Msi1 and Msi2, or targets unique to Msi1/*TRE-Msi1* or Msi2/*TRE-Msi2*, as well as targets bound by an unrelated RNA-binding protein Lin28b.

(H) Venn diagrams showing overlap in transcripts bound by endogenous Msi1 and Msi2 in wild-type crypts.

See also Figures S2–S4 and Tables S3, S4, S5, and S6.

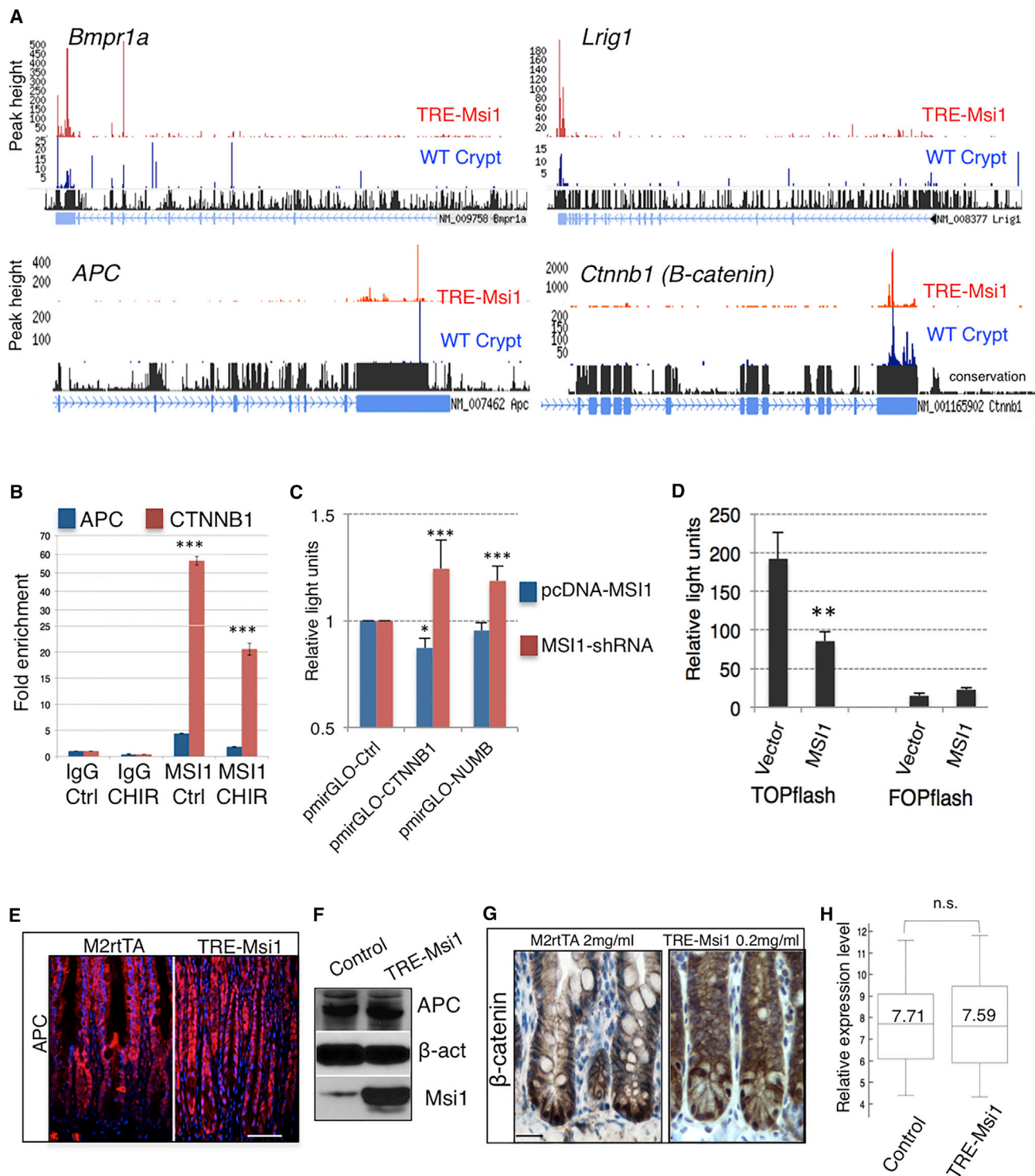


**Figure 4. Effects of Msi1 on Wnt Pathway Activity**

(A) CLIP-seq tracks showing endogenous (WT) and ectopically induced Msi1-binding target transcripts.  
(B) CLIP-qRT-PCR analysis of endogenous MSI1 binding to 3' UTRs of *APC* and *CTNNB1* (β-CATENIN) in HEK293 cells in the absence (Ctrl) or presence of the GSK3β inhibitor CHIR99021 (CHIR) (n = 3). \*\*\*p < 0.0005; Student's t test.  
(C) Luciferase reporter assays in HEK293 cells upon lentiviral shRNA knockdown of MSI1 (using pSico) or MSI1 overexpression (using pcDNA), shown for constructs containing the *CTNNB1* and *NUMB* 3' UTRs (n = 3; \*p < 0.05; \*\*\*p < 0.0005; Student's t test).

(legend continued on next page)

activation of the translational initiation factor eIF4E (Figure 5D). Examination of the levels and spatial distribution S6 phosphorylation (as an ultimate readout of S6 kinase activity downstream of mTORC1) revealed a dramatic induction and expansion throughout the entire epithelium upon Msi1 induction (Figures 5B and 5E). Thus, activation of the PDK1-AKT axis downstream of Pten by Msi1 contributes to the observed increase in mTORC1 activity in the intestinal epithelium. To confirm the functional importance of mTORC1 activity for the Msi1-driven phenotype, we pre-treated *TRE-Msi1* mice with rapamycin prior to inducing Msi1 with Dox. Rapamycin treatment blocked crypt fission, crypt height expansion, and hyperproliferation in the presence of ectopic Msi1 activity, confirming the functional importance of the mTORC1 complex downstream of Msi1 (Figures 5F–5H).

### Msi Activity Is Required for Intestinal Tumorigenesis

The data thus far establish that Msi1 activity is sufficient to transform the intestinal epithelium in a manner analogous to Msi2 and that these two RNA-binding proteins act on a similar set of target transcripts and affect analogous downstream pathways. If Msi1 and/or Msi2 act as oncoproteins in intestinal cancers, our data predict that the expression of one or the other would be sufficient to drive malignancy. We therefore assessed expression of *MSI1* and *MSI2* in a panel of human CRC cells and found that, whereas *MSI2* was consistently expressed across all cell lines, *MSI1* was coexpressed only in a subset and was frequently expressed at levels lower than those observed in normal human colon (Figure 6A). This pattern is precisely what we would predict from TCGA data analysis of paired tumor/adjacent normal tissue (Figure 1A; Wang et al., 2015). We thus inhibited MSI1 alone or in combination with MSI2 and/or  $\beta$ -CATENIN in several CRC cell lines. MSI1 inhibition alone had an antiproliferative effect in some lines, but not others (Figure 6B), and this effect could not be predicted by levels of *MSI1* expression relative to *MSI2*. Concomitant inhibition of both MSI1/MSI2 significantly inhibited growth of all cell lines analyzed, and additional inhibition of  $\beta$ -CATENIN blocked tumor cell growth more effectively than  $\beta$ -CATENIN or MSI inhibition alone (Figure 6B). Immunoblotting for MSI1 and nuclear (transcriptionally active)  $\beta$ -CATENIN indicates that MSI and  $\beta$ -CATENIN act in parallel pathways, as  $\beta$ -CATENIN knockdown has no major effect on MSI1 protein levels and vice versa (Figures 6C and S6A). We further confirmed that MSI inhibition abrogated the growth of tumor xenografts from RKO and HCT116 cells and that addition of  $\beta$ -CATENIN inhibition synergized with MSI inhibition to completely block tumor growth (Figures 7A–7D, S6B, and S6C).

These findings suggest that MSI activity is required for the maintenance of CRC growth. To test this in a more physiologically relevant setting and to address the importance for Msi ac-

tivity in tumor initiation, we examine tumorigenesis in genetic models of Msi loss in vivo. First, we generated compound *Msi1<sup>flox/flox</sup>::VillinCreER::APC<sup>min/+</sup>* (*Msi1<sup>-/-</sup>*), *Msi2<sup>flox/flox</sup>::VillinCreER::APC<sup>min/+</sup>* (*Msi2<sup>-/-</sup>*), and *Msi1<sup>flox/flox</sup>::Msi2<sup>flox/flox</sup>::VillinCreER::APC<sup>min/+</sup>* (*Msi-DKO*) mice enabling individual or concomitant ablation of the two *Msi* genes throughout the epithelium by tamoxifen-mediated activation of a *Villin-CreER* allele (el Marjou et al., 2004; Figures S7A–S7C). Acute deletion of *Msi1* in otherwise wild-type mice had no effect on *Msi2* expression and vice versa (Figure S7D). To study the effects of Msi loss on tumorigenesis, *Msi* genes were deleted alone or concomitantly followed by maintaining mice on a low protein diet to promote adenoma formation upon loss of heterozygosity at the *APC* locus. Individual deletion of either *Msi1* or *Msi2* had no effect of tumor burden in the *APC<sup>min</sup>* background (Figure S7E). In contrast, *MsiDKO* mice had a significant reduction in tumor burden relative to controls (Figure 7E). One hundred percent (68/68) of residual tumors forming in *MsiDKO* mice were found to have escaped recombination at one or more of the floxed *Msi* alleles, and thus *Msi<sup>-/-</sup>* tumors were never observed (Figure 7F). These data strongly indicate that Msi proteins act redundantly as oncogenes, with the presence of either Msi1 or Msi2 being sufficient to support tumorigenesis upon APC loss.

Whereas the *APC<sup>min/+</sup>* model is relevant to human disease in that spontaneous loss of APC is found in the vast majority of human CRC (Kinzler et al., 1991; Miyoshi et al., 1992; Nagase et al., 1992), the mouse model differs from the human condition in that tumors are primarily localized to the small intestine rather than colon, and they rarely progress to malignant adenocarcinoma. We therefore examined tumor formation in the AOM-DSS model of inflammation-driven colorectal adenocarcinoma (De Robertis et al., 2011). This model is clinically relevant as chronic inflammation is a leading indicator of CRC risk (van Hogezaand et al., 2002). Experimental and control mice were given a single dose of the mutagen azoxymethane (AOM), followed by cycles of the inflammatory agent dextran sodium sulfate (DSS) to drive formation of colorectal adenocarcinomas (Figure S7F). As expected, colorectal adenocarcinomas reproducibly formed in control mice (Figures 7G–7I and S7G). In contrast, *Msi-DKO* mice were completely resistant to tumorigenesis in this model with zero tumors forming (Figures 7G–7I and S7G). Taken together, our findings demonstrate the Msi1 and Msi2 act as potent, redundant oncoproteins whose activity is required for the initiation and maintenance of cancers of the intestinal epithelium.

### DISCUSSION

The Msi family of RNA-binding proteins has been implicated in oncogenic transformation in a number of organ systems, through

(D) Luciferase reporter assays in HCT116 cells for canonical Wnt pathway activation using the TOPflash reporter with multimerized  $\beta$ -catenin/TCF-binding sites upstream of luciferase or the control FOPflash reporter with mutated binding sites and empty vector or MSI1 overexpression ( $n = 3$ ; \*\* $p < 0.005$ ; Student's  $t$  test).

(E) Immunofluorescence staining of APC protein in control (*M2rtTA*) and *TRE-Msi1* mice 48 hr after Dox administration (scale = 100  $\mu$ m).

(F) Immunoblotting for APC in control (*M2rtTA*) and *TRE-Msi1* epithelium.

(G) Immunohistochemical staining for transcriptionally active (nuclear)  $\beta$ -catenin in crypts of control (*M2rtTA*) and *TRE-Msi1* transformed intestine (scale = 100  $\mu$ m).

(H) Box plot showing expression levels of known direct  $\beta$ -catenin target genes (full gene list in Experimental Procedures) in total intestinal epithelium from control (*M2rtTA*) and *TRE-Msi1* mice ( $n = 3$ ).



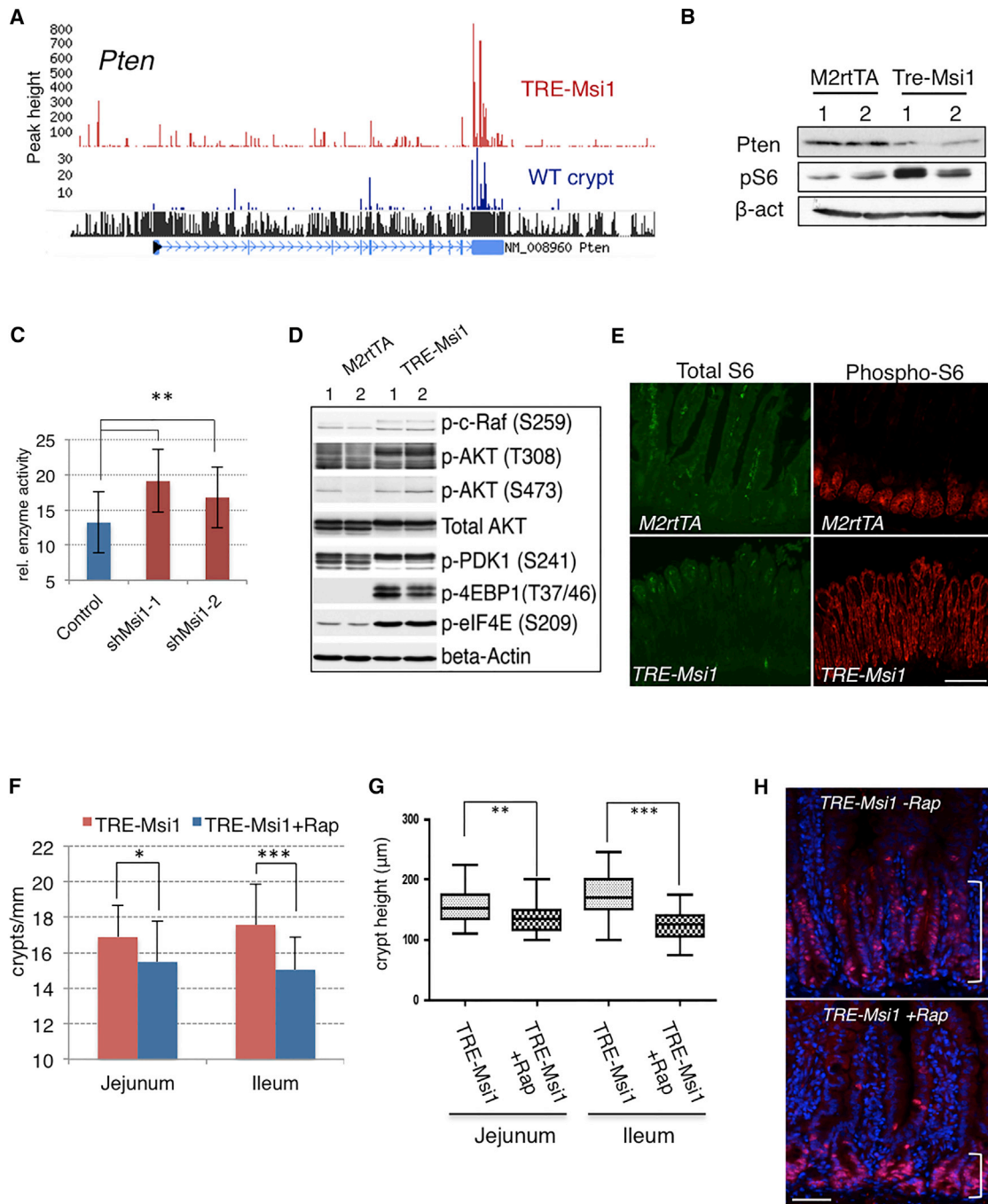


**Figure 5. Msi1 Functions Through the PDK-Akt-mTORC1 Axis**

(A) CLIP-seq track showing Msi1 binding to the 3' UTR of the *Pten* tumor suppressor mRNA.  
 (B) Immunoblotting for Pten and S6 phosphorylation upon Msi1 induction in the intestinal epithelium.  
 (C) PTEN enzymatic activity measured by immunoprecipitation followed by ELISA upon knockdown of MSI1 in 293T cells (\*\* $p < 0.005$ ; Student's *t* test).  
 (D) Immunoblot analysis of the PI3K-AKT-mTORC1 pathway downstream of Pten in the intestinal epithelium of two control and two *TRE-Msi1* mice treated with Dox for 24 hr.  
 (E) Immunofluorescence for phosphorylation of S6 by the mTORC1 target S6 kinase in control and *TRE-Msi1* transformed intestinal epithelium (scale = 200 μm).  
 (F–H) Rapamycin treatment rescues *TRE-Msi1*-induced transformation of the intestinal epithelium. Mice treated with rapamycin for 3 days prior to Dox administration exhibit decreased crypt fission (F) and a block in crypt height expansion (G; \* $p < 0.05$ ; \*\* $p < 0.005$ ; \*\*\* $p < 0.0005$ ; Student's *t* test). (H) Immunofluorescence staining for Ki67 of Dox-induced *TRE-Msi1* mice with or without rapamycin treatment (scale = 100 μm). Brackets indicate the height of the crypt proliferative zone.

See also Figure S5.

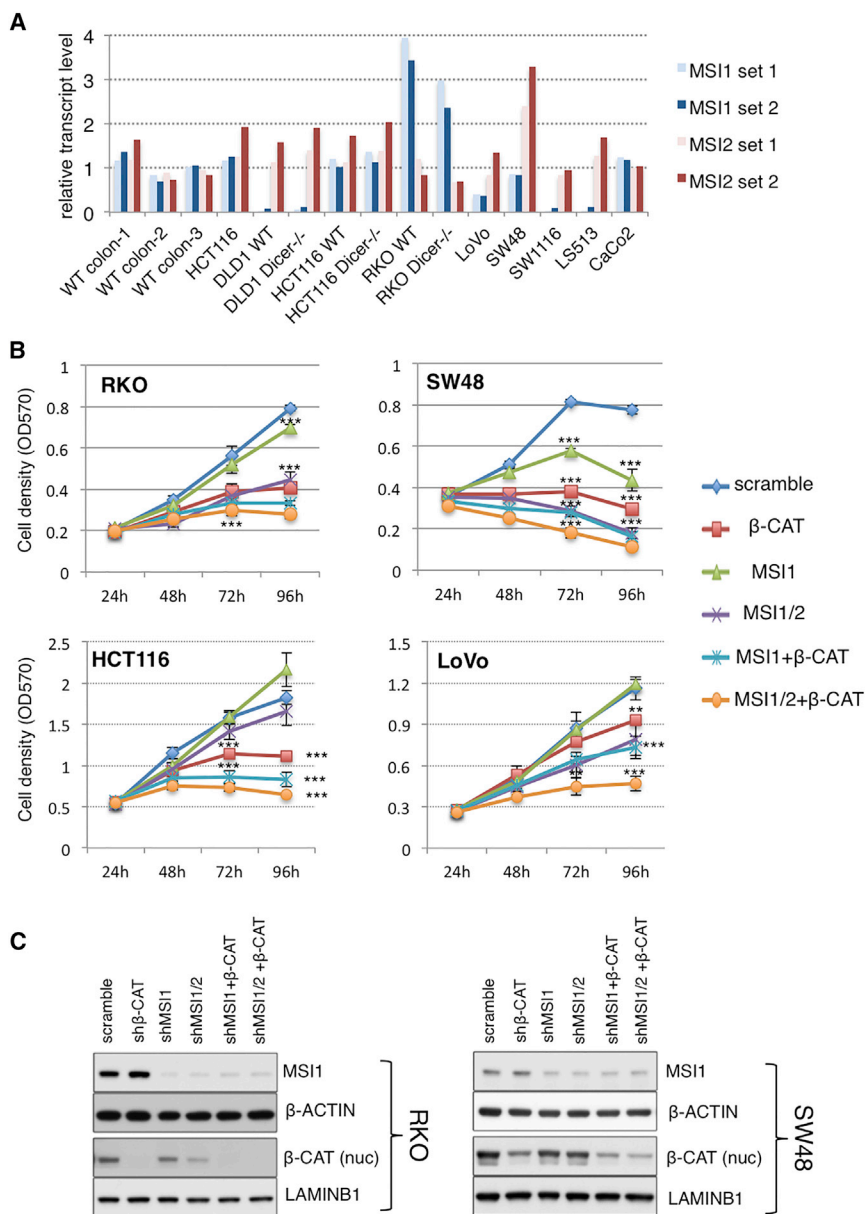


**Figure 6. MSI1 and MSI2 Promote Human Colorectal Cancer Cell Growth**

(A) Expression of *MSI1* and *MSI2* in three wild-type human colon biopsies and a panel of colorectal cancer cell lines, interrogated with two distinct primer sets for each *MSI* gene. HCT116 and HCT116 WT are the same cell line, procured from distinct sources (see [Experimental Procedures](#)).

(B) Growth of human colorectal cancer cell lines upon shRNA knockdown of *MSI1*, *MSI1* and *MSI2*, *MSI1* and  $\beta$ -CATENIN, and *MSI1* and 2 and  $\beta$ -CATENIN (\*\* $p < 0.005$ ; \*\*\* $p < 0.0005$ ; Student's  $t$  test).

(C) Immunoblotting validating knockdown of *MSI1* and transcriptionally active (nuclear)  $\beta$ -CATENIN in RKO and SW48 cells. Of note,  $\beta$ -CATENIN knockdown does not affect *MSI1* levels and *MSI1* knockdown does not significantly affect nuclear  $\beta$ -CATENIN levels.

See also [Figure S6](#).

emerged as a potent oncoprotein. In the hematopoietic system, *Msi2* is the only *Msi* family member expressed, and its activity is required for hematopoietic stem cell self-renewal ([Park et al., 2014](#)). Further, oncogenic *Msi2* activity promotes aggressive leukemias, in the context of acute myelogenous leukemia (AML), mixed-lineage leukemia (MLL), and chronic myelogenous leukemia (CML), where it drives chronic phase disease into the more-aggressive blast crisis phase characterized by a more stem-cell-like gene expression profile. Interestingly, in the hematopoietic system, the effects of *Msi2* appear to be largely independent of the previously identified *Msi1* RNA-binding targets encoding *Numb* and *p21* ([Kharas et al., 2010](#); [Park et al., 2014, 2015](#)). Rather, *Msi2* appears to be working through the TGF- $\beta$ , *Hoxa9*, *Ikzf2*, and *Myc* mRNAs, as well as through a more-general function in regulating RNA biogenesis in the hematopoietic lineage.

a number of proposed downstream mechanisms. In particular, several RNA-binding targets have been proposed to mediate the oncogenic function of *Msi1*, including the transcripts encoding *p21*, *Numb*, *APC*, and others ([Battelli et al., 2006](#); [Cambuli et al., 2015](#); [Imai et al., 2001](#); [Sanchez-Diaz et al., 2008](#); [Spears and Neufeld, 2011](#); [Sureban et al., 2008](#); [Uren et al., 2015](#); [Vo et al., 2012](#)). These mechanistic studies, however, were conducted using transformed cell lines in vitro or constitutive, random integrant gain-of-function transgenesis. In contrast, in vivo transcriptome-wide RNA binding analyses for *Msi1* and *Msi2* suggest that the reality is far more complex, with *Msi* interacting with hundreds to thousands of transcripts.

Although published studies have focused largely on *Msi1*, the second mammalian *Msi* family member, *Msi2* has recently

In the intestinal epithelium, *Msi2* governs RNA biogenesis and also has potent oncogenic properties consistent with observations in the hematopoietic system ([Wang et al., 2015](#)). In contrast to the hematopoietic system, however, *Msi2* bound to several transcripts encoding well-established colorectal tumor suppressors, including the negative regulator of ErbB-signaling *Lrig1*, as well as *Bmpr1a* and *Pten* ([Goel et al., 2004](#); [He et al., 2004, 2007](#); [Howe et al., 2001](#); [Marsh et al., 2008](#); [Naguib et al., 2011](#); [Powell et al., 2012](#); [Wang et al., 2015](#)). Interestingly, the known *Msi1*-binding targets encoding *p21* and *Numb* were found to bind *Msi2* in vivo; however, *Msi2* induction does not elicit a strong up-regulation of the Notch pathway, nor does *Msi2* potentiate activity of the canonical Wnt pathway as proposed for *Msi1* in cell culture models. Instead, the major oncogenic effects of *Msi2* in vivo

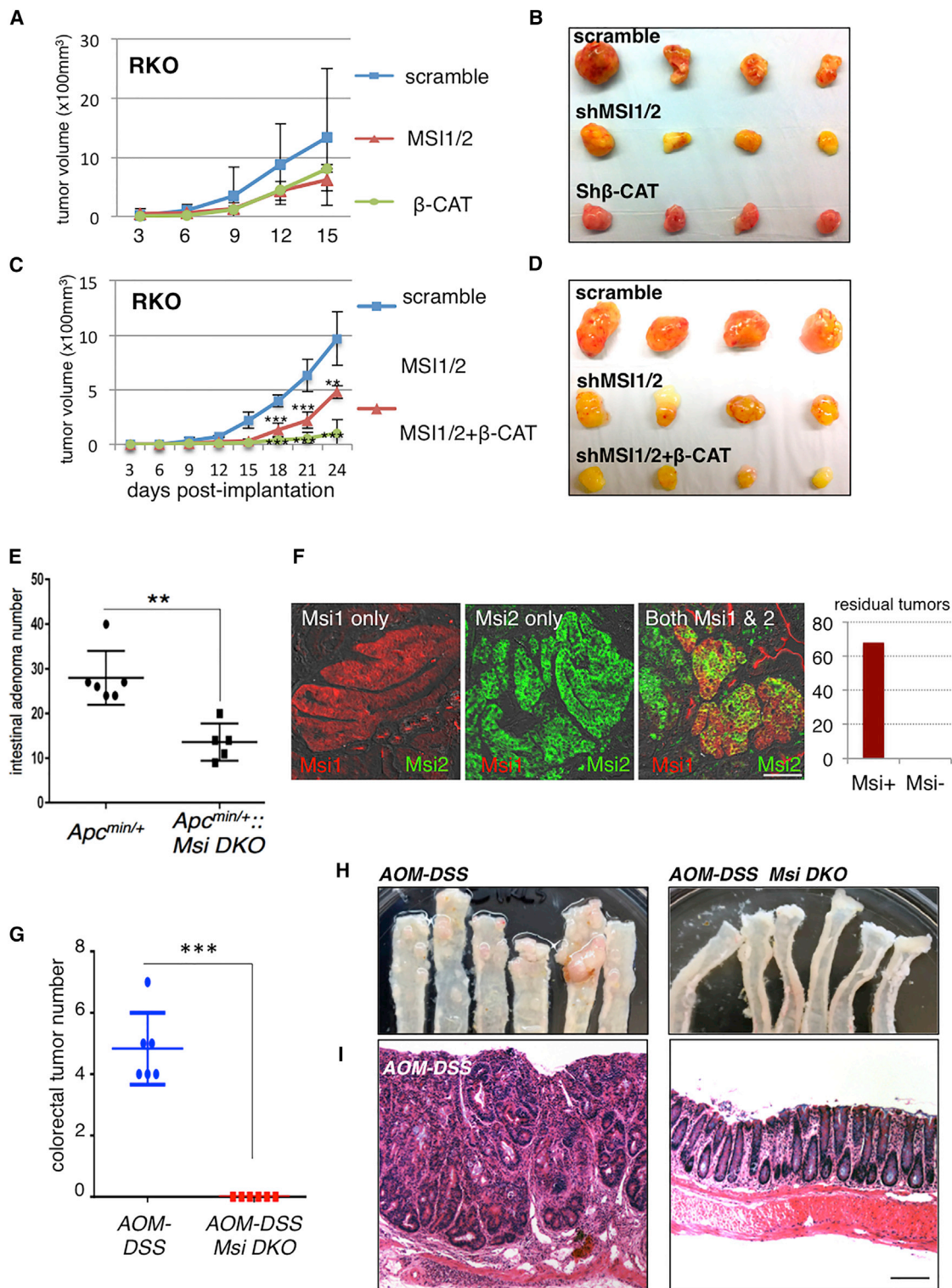


**Figure 7. MSI1/Msi1 and MSI2/Msi2 Cooperate to Promote Tumor Growth In Vivo**

(A and B) Growth of RKO cell xenografts upon MSI or β-CATENIN shRNA knockdown (A), with tumors shown after dissection upon termination of the experiment (B).

(C and D) Growth of RKO cell xenografts upon combined knockdown of MSI proteins alone or with β-CATENIN knockdown (C), with tumors shown after dissection upon termination of the experiment (D; \*\*p < 0.005; \*\*\*p < 0.0005; Student's t test).

(legend continued on next page)



appears to be activation of mTORC1, a complex dispensable for intestinal function but known to be required for intestinal tumorigenesis downstream of APC loss (Faller et al., 2015; Fujishita et al., 2008). Thus, there exist discrepancies between the proposed oncogenic functions of Msi1 in CRC cells (e.g., suppression of p21, Numb, and APC translation and potentiation of Wnt signaling) and the acute oncogenic consequences of Msi2 gain of function in vivo (RNA metabolism and mTORC1 activation). Whether these discrepancies represent actual biological differences between the activity of the two Msi family members or differences between the in vitro and in vivo model systems were not understood.

Here, we generated a single-copy, inducible Msi1 mouse model using genetic loci and strains identical to those previously used for Msi2 induction in vivo, enabling a direct comparison of the oncogenic consequences of acute gain of function of the two Msi family members. Remarkably, Msi1 induction elicits the identical phenotypic transformation of the intestinal epithelium observed for Msi2 through interaction with a largely common repertoire of transcripts. Interestingly, we observed that Msi1 did bind to the APC mRNA as reported in vitro; however, we observed a stronger interaction between Msi1 and the Ctnnb1 mRNA, suggesting that Msi1 might regulate the canonical Wnt pathway. However, in contrast to prior reports, we found no evidence that Msi1 potentiates Wnt pathway activity either in vitro or in vivo, using either human or mouse MSI1/Msi1, consistent with our observation that MSI1/2 knockdown in human CRC cells does not significantly affect levels of nuclear  $\beta$ -CATENIN. Further, the observation that  $\beta$ -CATENIN knockdown does not affect MSI levels supports a model in which the oncogenic activities of MSI and  $\beta$ -CATENIN lie in parallel pathways.

These data indicate that Msi1 and Msi2 function redundantly, leading to the prediction that Msi proteins can act interchangeably as oncogenes in CRC. Indeed, dual inhibition of both MSI proteins is required to fully abrogate tumor growth in CRC cell lines. Interestingly, the dependence of these cells on MSI activity appears to be independent of underlying genetic driver mutations, as MSI inhibition was effective in blocking growth of RKO cells (mutations in BRAF, PIK3CA, and microsatellite instability), SW48 cells (mutations in APC and microsatellite instability), HCT116 (mutations in KRAS, PIK3CA, TP53,  $\beta$ -CATENIN, and microsatellite instability), and LoVo cells (mutations in KRAS, APC, and microsatellite instability; Ahmed et al., 2013). This observation is similar to what was previously observed for MSI2 in human leukemias, where MSI2 upregulation and subsequent oncogene addiction occurs regardless of underlying genetic mutation (Kharas et al., 2010).

Further, despite the focus on MSI1 in CRC, our data suggest that MSI2 may be the dominant MSI family member in driving these malignancies, as MSI2 upregulation is essentially ubiquitous in CRC, whereas MSI1 upregulation is observed only in a subset of human tumor samples and CRC cell lines. Why MSI2 is preferentially expressed relative to MSI1 remains unclear.

Ultimately, the current study demonstrates that both Msi family members elicit an analogous transformation of the intestinal epithelium, with identical phenotypic changes, highly similar gene expression profiles, and overlapping RNA-binding targets. Further, concomitant loss of both Msi family members was sufficient to abrogate tumorigenesis in both human and murine models, clearly demonstrating the critical importance of these RNA-binding proteins to the ontogeny of CRCs. Our findings serve as a basis for exploring the mechanisms through which MSI proteins promote human cancers and highlight the critical importance of addressing the role of both family members when studying MSI function and consideration of their redundant function for development of MSI inhibitors.

## EXPERIMENTAL PROCEDURES

### Generation of TRE-Msi1 Mice

All procedures involving mice were reviewed and approved by the Institutional Animal Care and Use Committee of the University of Pennsylvania (Animal Welfare Assurance reference number A3079-01; approved protocol no. 803415 granted to Dr. Lengner) and were in accordance with the guidelines set forth in the Guide for the Care and Use of Laboratory Animals of the National Research Council of the NIH. Euthanasia was performed using controlled flow carbon dioxide administration followed by cervical dislocation.

The murine *Msi1* cDNA (a kind gift from Dr. Joseph Verdi, Maine Medical Center Research Institute) was cloned into the unique EcoRI restriction site of the pBS31 vector containing a PGK promoter followed by an ATG start codon and an FRT recombination site, followed by a splice acceptor-double polyA cassette, the tetracycline operator with a minimal CMV promoter, the unique EcoRI site, and an SV40 polyadenylation signal. The pBS31-Msi1 vector was then electroporated along with a Flpe recombinase-expressing vector into KH2 embryonic stem cells harboring the modified reverse tetracycline transactivator (*M2rtTA*) targeted to and under transcriptional control of the *ROSA26* locus, as well as an FRT-flanked *PGK-neomycinR* cassette followed by a promoterless, ATG-less hygromycinR cassette targeted downstream of the *Collagen1a1* locus. Selection for hygromycin resistance upon flip-in yielded numerous colonies that were verified for proper recombination at the *Coll1a1* locus by digestion of genomic DNA and Southern blotting with a 3' internal probe, yielding a 6.2-kb wild-type band, a 6.7-kb band for the FRT-containing knockin allele, and a 4.1-kb band for the successfully flipped-in Msi1-inducible allele (*TRE-Msi1*).

### CLIP-Seq and CLIP-qRT-PCR

CLIP-seq libraries were made as previously described in Chi et al. (2009) with modifications. The CLIP-seq procedure used in this study was identical to that

(E) Frequency of intestinal adenomas in *APC<sup>min/+</sup>* mice with or without deletion of *Msi* gene deletion in *Msi1/2<sup>flox/flox</sup>::Villin-CreER::APC<sup>min/+</sup>* mice (\*\*p < 0.005; Student's t test; n = 5–6 mice per group).

(F) Representative immunofluorescence micrographs of residual tumors in *Msi1/2<sup>flox/flox</sup>::Villin-CreER::APC<sup>min/+</sup>* mice showing Msi1 (red), Msi2 (green), or Msi1/2 expression (scale = 100  $\mu$ m). The graph at right depicts number of residual tumors in *Msi1/2<sup>flox/flox</sup>::Villin-CreER::APC<sup>min/+</sup>* that were either positive or negative for Msi immunoreactivity (100% or 68/68 total residual tumors scored positive).

(G) Frequency of inflammation-driven colorectal adenomas/adenocarcinomas in mice treated with the AOM-DSS protocol, with or without prior *Msi* gene deletion in *Msi1/2<sup>flox/flox</sup>::Villin-CreER* mice (\*\*\*p < 0.0005; Student's t test; n = 6 mice per group).

(H) Photographs of distal colon resected from control (left) and *Msi1/2* double knockout (right) mice at the end of the AOM-DSS protocol.

(I) Representative H&E histological section of a colorectal adenocarcinoma resulting from AOM-DSS treatment in control mice (left). In contrast, mice lacking Msi gene function exhibited normal colon morphology after the AOM-DSS protocol (right; scale = 200  $\mu$ m).

See also Figure S7.

used in Wang et al. (2015) and is described in detail in the Supplemental Experimental Procedures.

### Generation and Verification of Msi Floxed Alleles

*Msi1* and *Msi2* alleles were targeted using homologous recombination in V6.5 embryonic stem cells. Generation of the *Msi2* conditional allele is described in Park et al. (2014). Targeted (3-lox) clones were isolated after neomycin (G418) selection, and Southern blotting using external probes flanking both the 3' and 5' targeting arm validated proper insertion of the targeting vector. Three-lox clones were then transiently electroporated with Cre recombinase and subcloned to identify 2-lox conditional clones. Clones harboring 2-lox (floxed) *Msi1* and *Msi2* alleles were injected into blastocysts and resulting chimeras backcrossed to a Black/6 background. Addition of Cre recombinase (either transiently in culture or through intercrossing with *Villin-CreER* mice) resulted in deletion of the transcriptional start site and exons 1 and 2 (in the case of *Msi1*) or exons 1–4 (in the case of *Msi2*), generating a 1-lox-null allele that was validated by Southern blotting and Msi protein loss. Southern blotting was carried out by digesting genomic DNA overnight, transferring to Hybond XL membrane (Amersham/GE Healthcare) and hybridizing with a <sup>32</sup>P-probe labeled by random priming (Prime-it II, Agilent Technologies) in Church buffer at 60°C overnight followed by washing with increasing stringency SDS/SSC buffer and exposure to film.

For *Msi1/2* in vivo expression analysis in Figure S7D, *Msi1<sup>flox/flox</sup>::VillinCreER* or *Msi2<sup>flox/flox</sup>::VillinCreER* mice were administered five doses of tamoxifen (2 mg/dose in 100  $\mu$ l corn oil) when they were 6 weeks old. After a 5-day chase period, crypt epithelial RNA was isolated and *Msi* gene expression was analyzed.

### Apc<sup>min/+</sup> and AOM-DSS Tumor Models

The *Apc<sup>min/+</sup>* mice were obtained from JAX lab (stock number: 002020). *Apc<sup>min/+</sup>::Msi1/2<sup>flox/flox</sup>*, *Apc<sup>min/+</sup>::Msi1<sup>flox/flox</sup>*, or *Apc<sup>min/+</sup>::Msi2<sup>flox/flox</sup>* mice (n = 6–7 mice per group) with or without the *Villin-CreER* allele (el Marjou et al., 2004) were given five doses of tamoxifen (2 mg/dose in 100  $\mu$ l corn oil) when they were 6 weeks old and then raised on a low-protein/high-fat diet (Research Diets; D12079B) for 6 months. Additional series of tamoxifen doses was given 2 and 4 months post-initiation of high-fat diet to maximize recombination of floxed *Msi* alleles. Adenomas were scored by two independent researchers using a stereomicroscope for *Apc<sup>min/+</sup>::Msi1/2<sup>flox/flox</sup>* or scored histologically for *Apc<sup>min/+</sup>::Msi1<sup>flox/flox</sup>* or *Apc<sup>min/+</sup>::Msi2<sup>flox/flox</sup>* mice.

For AOM-DSS, control mice were co-housed with experimental mice and injected with 100  $\mu$ l of 20 mg/ml<sup>-1</sup> tamoxifen every day for 5 days (n = 6 mice per group). Two weeks after the final tamoxifen injection, all mice were given a single intraperitoneal injection of 10 mg/kg<sup>-1</sup> of AOM. One week later, all mice received 3% DSS in their drinking water for 7 days and then regular water for 14 days. Two more cycles of DSS were subsequently administered, with the third and final cycle reduced to 2.5% DSS. Fecal samples were collected regularly during the experiment, and mice were observed daily and weighed weekly. Mice were sacrificed approximately 5 weeks after the last DSS cycle. Tumors were counted using a stereomicroscope, and colon tissue was subsequently fixed for histology.

### ACCESSION NUMBERS

The accession number for the transcriptome profiles reported in this paper is GEO: GSE74321. The accession number for the CLIP-seq data reported in this paper is GEO: GSE54598.

### SUPPLEMENTAL INFORMATION

Supplemental Information includes Supplemental Experimental Procedures, seven figures, and six tables and can be found with this article online at <http://dx.doi.org/10.1016/j.celrep.2015.11.022>.

### AUTHOR CONTRIBUTIONS

N.L., Z.Y., and C.J.L. designed all experiments, executed the majority of experiments, and wrote the manuscript. M.Y. performed histological and flow cy-

tometric analysis. A.N.-D. performed colorectal-tumor-modeling experiments. F.L., L.V., A.S.N., R.J.C., and B.D.G. performed analysis of sequencing data. K.P. and A.N.-D. managed animal colonies and performed luciferase assays. D.-H.W. performed human patient sample expression analysis. S.W. performed histological analysis. S.R., J.T., and S.T.J. performed analysis of transcriptome profiling data. G.M. performed electrophoretic mobility shift assays. M.G.K. and C.J.L. generated *TRE-Msi1*, *Msi1<sup>flox/flox</sup>*, and *Msi2<sup>flox/flox</sup>* mouse strains. T.S.B. performed husbandry with these strains. M.G.K. contributed to editing the manuscript. A.V. and P.S.K. contributed to the conception of mTorC1-related experiments and mTorC1 pathway analysis as well as reagents. R.P.D. contributed to the development and application of the in vivo CLIP-seq procedures. K.Y. performed TCGA data analysis. S.S. performed histological analysis and quantification.

### ACKNOWLEDGMENTS

We thank members of the University of Pennsylvania Functional Genomics Core, particularly Dr. Jonathan Schug, for assistance with massively parallel sequencing. We thank Drs. Anil Rustgi, John Lynch, and Kathryn Hamilton in the Division of Gastroenterology as well as members of Dr. Igor Brodsky's lab in the Department of Pathobiology for reagents and fruitful discussions. M.Y. is funded by a Howard Hughes international student research fellowship. Z.Y. is funded by National Natural Science Foundation of China (NSFC; 81572614) and the National Basic Research Program of China (973 program-2011CB944103 and 2015SKLAB6-16). C.J.L. is funded by a fellowship from the W.W. Smith Charitable Trust, a pilot award from an American Cancer Society Institutional Research Grant, a grant from the Pennsylvania Department of Health (Health Research Formula Fund no. 4100054874), and R01 CA168654 from the National Cancer Institute. This work was supported in part by the NIH/NIDDK Center for Molecular Studies in Digestive and Liver Diseases (NIH-P30-DK050306) and its core facilities, and C.J.L. was supported by the center's pilot and feasibility grant program.

Received: April 15, 2015

Revised: September 8, 2015

Accepted: November 4, 2015

Published: December 3, 2015

### REFERENCES

- Ahmed, D., Eide, P.W., Eilertsen, I.A., Danielsen, S.A., Eknæs, M., Hektoen, M., Lind, G.E., and Lothe, R.A. (2013). Epigenetic and genetic features of 24 colon cancer cell lines. *Oncogenesis* 2, e71.
- Barker, N., van Es, J.H., Kuipers, J., Kujala, P., van den Born, M., Cozijnsen, M., Haegebarth, A., Korving, J., Begthel, H., Peters, P.J., and Clevers, H. (2007). Identification of stem cells in small intestine and colon by marker gene *Lgr5*. *Nature* 449, 1003–1007.
- Battelli, C., Nikopoulos, G.N., Mitchell, J.G., and Verdi, J.M. (2006). The RNA-binding protein Musashi-1 regulates neural development through the translational repression of p21WAF-1. *Mol. Cell. Neurosci.* 31, 85–96.
- Cambuli, F.M., Correa, B.R., Rezza, A., Burns, S.C., Qiao, M., Uren, P.J., Kress, E., Boussouar, A., Galante, P.A., Penalva, L.O., et al. (2015). A mouse model of targeted Musashi1 expression in whole intestinal epithelium suggests regulatory roles in cell cycle and stemness. *Stem Cells*, Published online August 25, 2015. <http://dx.doi.org/10.1002/stem.2202>.
- Chi, S.W., Zang, J.B., Mele, A., and Darnell, R.B. (2009). Argonaute HITS-CLIP decodes microRNA-mRNA interaction maps. *Nature* 460, 479–486.
- Clarke, R.B., Anderson, E., Howell, A., and Potten, C.S. (2003). Regulation of human breast epithelial stem cells. *Cell Prolif.* 36 (Suppl 1), 45–58.
- De Robertis, M., Massi, E., Poeta, M.L., Carotti, S., Morini, S., Cecchetelli, L., Signori, E., and Fazio, V.M. (2011). The AOM/DSS murine model for the study of colon carcinogenesis: From pathways to diagnosis and therapy studies. *J. Carcinog.* 10, 9.
- de Sousa Abreu, R., Sanchez-Diaz, P.C., Vogel, C., Burns, S.C., Ko, D., Burton, T.L., Vo, D.T., Chennasamudaram, S., Le, S.Y., Shapiro, B.A., and

- Penalva, L.O. (2009). Genomic analyses of musashi1 downstream targets show a strong association with cancer-related processes. *J. Biol. Chem.* 284, 12125–12135.
- el Marjou, F., Janssen, K.P., Chang, B.H., Li, M., Hindie, V., Chan, L., Louvard, D., Chambon, P., Metzger, D., and Robine, S. (2004). Tissue-specific and inducible Cre-mediated recombination in the gut epithelium. *Genesis* 39, 186–193.
- Faller, W.J., Jackson, T.J., Knight, J.R., Ridgway, R.A., Jamieson, T., Karim, S.A., Jones, C., Radulescu, S., Huels, D.J., Myant, K.B., et al. (2015). mTORC1-mediated translational elongation limits intestinal tumour initiation and growth. *Nature* 517, 497–500.
- Fujishita, T., Aoki, K., Lane, H.A., Aoki, M., and Taketo, M.M. (2008). Inhibition of the mTORC1 pathway suppresses intestinal polyp formation and reduces mortality in ApcDelta716 mice. *Proc. Natl. Acad. Sci. USA* 105, 13544–13549.
- Goel, A., Arnold, C.N., Niedzwiecki, D., Carethers, J.M., Dowell, J.M., Wasserman, L., Compton, C., Mayer, R.J., Bertagnolli, M.M., and Boland, C.R. (2004). Frequent inactivation of PTEN by promoter hypermethylation in microsatellite instability-high sporadic colorectal cancers. *Cancer Res.* 64, 3014–3021.
- He, X.C., Zhang, J., Tong, W.G., Tawfik, O., Ross, J., Scoville, D.H., Tian, Q., Zeng, X., He, X., Wiedemann, L.M., et al. (2004). BMP signaling inhibits intestinal stem cell self-renewal through suppression of Wnt-beta-catenin signaling. *Nat. Genet.* 36, 1117–1121.
- He, X.C., Yin, T., Grindley, J.C., Tian, Q., Sato, T., Tao, W.A., Dirisina, R., Porter-Westpfahl, K.S., Hembree, M., Johnson, T., et al. (2007). PTEN-deficient intestinal stem cells initiate intestinal polyposis. *Nat. Genet.* 39, 189–198.
- Howe, J.R., Bair, J.L., Sayed, M.G., Anderson, M.E., Mitros, F.A., Petersen, G.M., Velculescu, V.E., Traverso, G., and Vogelstein, B. (2001). Germline mutations of the gene encoding bone morphogenetic protein receptor 1A in juvenile polyposis. *Nat. Genet.* 28, 184–187.
- Imai, T., Tokunaga, A., Yoshida, T., Hashimoto, M., Mikoshiba, K., Weinmaster, G., Nakafuku, M., and Okano, H. (2001). The neural RNA-binding protein Musashi1 translationally regulates mammalian numb gene expression by interacting with its mRNA. *Mol. Cell. Biol.* 21, 3888–3900.
- Ito, T., Kwon, H.Y., Zimdahl, B., Congdon, K.L., Blum, J., Lento, W.E., Zhao, C., Lagoo, A., Gerrard, G., Feroni, L., et al. (2010). Regulation of myeloid leukaemia by the cell-fate determinant Musashi. *Nature* 466, 765–768.
- Katz, Y., Li, F., Lambert, N.J., Sokol, E.S., Tam, W.L., Cheng, A.W., Airolidi, E.M., Lengner, C.J., Gupta, P.B., Yu, Z., et al. (2014). Musashi proteins are post-transcriptional regulators of the epithelial-luminal cell state. *eLife* 3, e03915.
- Kawahara, H., Imai, T., Imataka, H., Tsujimoto, M., Matsumoto, K., and Okano, H. (2008). Neural RNA-binding protein Musashi1 inhibits translation initiation by competing with eIF4G for PABP. *J. Cell Biol.* 181, 639–653.
- Kayahara, T., Sawada, M., Takaishi, S., Fukui, H., Seno, H., Fukuzawa, H., Suzuki, K., Hiai, H., Kageyama, R., Okano, H., and Chiba, T. (2003). Candidate markers for stem and early progenitor cells, Musashi-1 and Hes1, are expressed in crypt base columnar cells of mouse small intestine. *FEBS Lett.* 535, 131–135.
- Kharas, M.G., Lengner, C.J., Al-Shahrour, F., Bullinger, L., Ball, B., Zaidi, S., Morgan, K., Tam, W., Paktinat, M., Okabe, R., et al. (2010). Musashi-2 regulates normal hematopoiesis and promotes aggressive myeloid leukemia. *Nat. Med.* 16, 903–908.
- Kinzler, K.W., Nilbert, M.C., Su, L.K., Vogelstein, B., Bryan, T.M., Levy, D.B., Smith, K.J., Preisinger, A.C., Hedge, P., McKechnie, D., et al. (1991). Identification of FAP locus genes from chromosome 5q21. *Science* 253, 661–665.
- Levin, T.G., Powell, A.E., Davies, P.S., Silk, A.D., Dismuke, A.D., Anderson, E.C., Swain, J.R., and Wong, M.H. (2010). Characterization of the intestinal cancer stem cell marker CD166 in the human and mouse gastrointestinal tract. *Gastroenterology* 139, 2072–2082.e5.
- Li, D., Peng, X., Yan, D., Tang, H., Huang, F., Yang, Y., and Peng, Z. (2011). Msi-1 is a predictor of survival and a novel therapeutic target in colon cancer. *Ann. Surg. Oncol.* 18, 2074–2083.
- Li, N., Yousefi, M., Nakauka-Ddamba, A., Jain, R., Tobias, J., Epstein, J.A., Jensen, S.T., and Lengner, C.J. (2014). Single-cell analysis of proxy reporter allele-marked epithelial cells establishes intestinal stem cell hierarchy. *Stem Cell Rep.* 3, 876–891.
- Madison, B.B., Liu, Q., Zhong, X., Hahn, C.M., Lin, N., Emmett, M.J., Stanger, B.Z., Lee, J.-S., and Rustgi, A.K. (2013). LIN28B promotes growth and tumorigenesis of the intestinal epithelium via Let-7. *Genes Dev.* 27, 2233–2245.
- Marsh, V., Winton, D.J., Williams, G.T., Dubois, N., Trumpp, A., Sansom, O.J., and Clarke, A.R. (2008). Epithelial Pten is dispensable for intestinal homeostasis but suppresses adenoma development and progression after Apc mutation. *Nat. Genet.* 40, 1436–1444.
- Miyoshi, Y., Nagase, H., Ando, H., Horii, A., Ichii, S., Nakatsuru, S., Aoki, T., Miki, Y., Mori, T., and Nakamura, Y. (1992). Somatic mutations of the APC gene in colorectal tumors: mutation cluster region in the APC gene. *Hum. Mol. Genet.* 1, 229–233.
- Nagase, H., Miyoshi, Y., Horii, A., Aoki, T., Petersen, G.M., Vogelstein, B., Maher, E., Ogawa, M., Maruyama, M., Utsunomiya, J., et al. (1992). Screening for germ-line mutations in familial adenomatous polyposis patients: 61 new patients and a summary of 150 unrelated patients. *Hum. Mutat.* 1, 467–473.
- Naguib, A., Cooke, J.C., Happerfield, L., Kerr, L., Gay, L.J., Luben, R.N., Ball, R.Y., Mitrou, P.N., McTaggart, A., and Arends, M.J. (2011). Alterations in PTEN and PIK3CA in colorectal cancers in the EPIC Norfolk study: associations with clinicopathological and dietary factors. *BMC Cancer* 11, 123.
- Nakamura, M., Okano, H., Blendy, J.A., and Montell, C. (1994). Musashi, a neural RNA-binding protein required for Drosophila adult external sensory organ development. *Neuron* 13, 67–81.
- Okabe, M., Imai, T., Kurusu, M., Hiromi, Y., and Okano, H. (2001). Translational repression determines a neuronal potential in Drosophila asymmetric cell division. *Nature* 411, 94–98.
- Okano, H., Imai, T., and Okabe, M. (2002). Musashi: a translational regulator of cell fate. *J. Cell. Sci.* 115, 1355–1359.
- Park, S.M., Deering, R.P., Lu, Y., Tivnan, P., Lianoglou, S., Al-Shahrour, F., Ebert, B.L., Hacohen, N., Leslie, C., Daley, G.Q., et al. (2014). Musashi-2 controls cell fate, lineage bias, and TGF- $\beta$  signaling in HSCs. *J. Exp. Med.* 211, 71–87.
- Park, S.M., Gönen, M., Vu, L., Minuesa, G., Tivnan, P., Barlowe, T.S., Taggart, J., Lu, Y., Deering, R.P., Hacohen, N., et al. (2015). Musashi2 sustains the mixed-lineage leukemia-driven stem cell regulatory program. *J. Clin. Invest.* 125, 1286–1298.
- Potten, C.S., Booth, C., Tudor, G.L., Booth, D., Brady, G., Hurley, P., Ashton, G., Clarke, R., Sakakibara, S., and Okano, H. (2003). Identification of a putative intestinal stem cell and early lineage marker; musashi-1. *Differentiation* 71, 28–41.
- Powell, A.E., Wang, Y., Li, Y., Poulin, E.J., Means, A.L., Washington, M.K., Higinbotham, J.N., Juchheim, A., Prasad, N., Levy, S.E., et al. (2012). The pan-ErbB negative regulator Lrig1 is an intestinal stem cell marker that functions as a tumor suppressor. *Cell* 149, 146–158.
- Rezza, A., Skah, S., Roche, C., Nadjar, J., Samarut, J., and Plateroti, M. (2010). The overexpression of the putative gut stem cell marker Musashi-1 induces tumorigenesis through Wnt and Notch activation. *J. Cell Sci.* 123, 3256–3265.
- Sakakibara, S., Nakamura, Y., Yoshida, T., Shibata, S., Koike, M., Takano, H., Ueda, S., Uchiyama, Y., Noda, T., and Okano, H. (2002). RNA-binding protein Musashi family: roles for CNS stem cells and a subpopulation of ependymal cells revealed by targeted disruption and antisense ablation. *Proc. Natl. Acad. Sci. USA* 99, 15194–15199.
- Sanchez-Diaz, P.C., Burton, T.L., Burns, S.C., Hung, J.Y., and Penalva, L.O. (2008). Musashi1 modulates cell proliferation genes in the medulloblastoma cell line Daoy. *BMC Cancer* 8, 280.
- Sansom, O.J., Reed, K.R., Hayes, A.J., Ireland, H., Brinkmann, H., Newton, I.P., Batlle, E., Simon-Assmann, P., Clevers, H., Nathke, I.S., et al. (2004). Loss of Apc in vivo immediately perturbs Wnt signaling, differentiation, and migration. *Genes Dev.* 18, 1385–1390.



- Spears, E., and Neufeld, K.L. (2011). Novel double-negative feedback loop between adenomatous polyposis coli and Musashi1 in colon epithelia. *J. Biol. Chem.* **286**, 4946–4950.
- Subramanian, A., Tamayo, P., Mootha, V.K., Mukherjee, S., Ebert, B.L., Gillette, M.A., Paulovich, A., Pomeroy, S.L., Golub, T.R., Lander, E.S., et al. (2005). Gene set enrichment analysis: a knowledge-based approach for interpreting genome-wide expression profiles. *Proc. Natl. Acad. Sci. USA* **102**, 15545–15550.
- Sugiyama-Nakagiri, Y., Akiyama, M., Shibata, S., Okano, H., and Shimizu, H. (2006). Expression of RNA-binding protein Musashi in hair follicle development and hair cycle progression. *Am. J. Pathol.* **168**, 80–92.
- Sureban, S.M., May, R., George, R.J., Dieckgraefe, B.K., McLeod, H.L., Ramalingam, S., Bishnupuri, K.S., Natarajan, G., Anant, S., and Houchen, C.W. (2008). Knockdown of RNA binding protein musashi-1 leads to tumor regression in vivo. *Gastroenterology* **134**, 1448–1458.
- Sutherland, J.M., Fraser, B.A., Sobinoff, A.P., Pye, V.J., Davidson, T.L., Siddall, N.A., Koopman, P., Hime, G.R., and McLaughlin, E.A. (2014). Developmental expression of Musashi-1 and Musashi-2 RNA-binding proteins during spermatogenesis: analysis of the deleterious effects of dysregulated expression. *Biol. Reprod.* **90**, 92.
- Uren, P.J., Vo, D.T., de Araujo, P.R., Pötschke, R., Burns, S.C., Bahrami-Samani, E., Qiao, M., de Sousa Abreu, R., Nakaya, H.I., Correa, B.R., et al. (2015). RNA-binding protein Musashi1 is a central regulator of adhesion pathways in glioblastoma. *Mol. Cell. Biol.* **35**, 2965–2978.
- van Hogezaand, R.A., Eichhorn, R.F., Choudry, A., Veenendaal, R.A., and Lamers, C.B. (2002). Malignancies in inflammatory bowel disease: fact or fiction? *Scand. J. Gastroenterol. Suppl.*, 48–53.
- Vo, D.T., Subramaniam, D., Remke, M., Burton, T.L., Uren, P.J., Gelfond, J.A., de Sousa Abreu, R., Burns, S.C., Qiao, M., Suresh, U., et al. (2012). The RNA-binding protein Musashi1 affects medulloblastoma growth via a network of cancer-related genes and is an indicator of poor prognosis. *Am. J. Pathol.* **181**, 1762–1772.
- Wang, X.Y., Yin, Y., Yuan, H., Sakamaki, T., Okano, H., and Glazer, R.I. (2008). Musashi1 modulates mammary progenitor cell expansion through proliferin-mediated activation of the Wnt and Notch pathways. *Mol. Cell. Biol.* **28**, 3589–3599.
- Wang, S., Li, N., Yousefi, M., Nakauka-Ddamba, A., Li, F., Parada, K., Rao, S., Minuesa, G., Katz, Y., Gregory, B.D., et al. (2015). Transformation of the intestinal epithelium by the MSI2 RNA-binding protein. *Nat. Commun.* **6**, 6517.
- Wasan, H.S., Park, H.S., Liu, K.C., Mandir, N.K., Winnett, A., Sasieni, P., Bodmer, W.F., Goodlad, R.A., and Wright, N.A. (1998). APC in the regulation of intestinal crypt fission. *J. Pathol.* **185**, 246–255.

Cell Reports

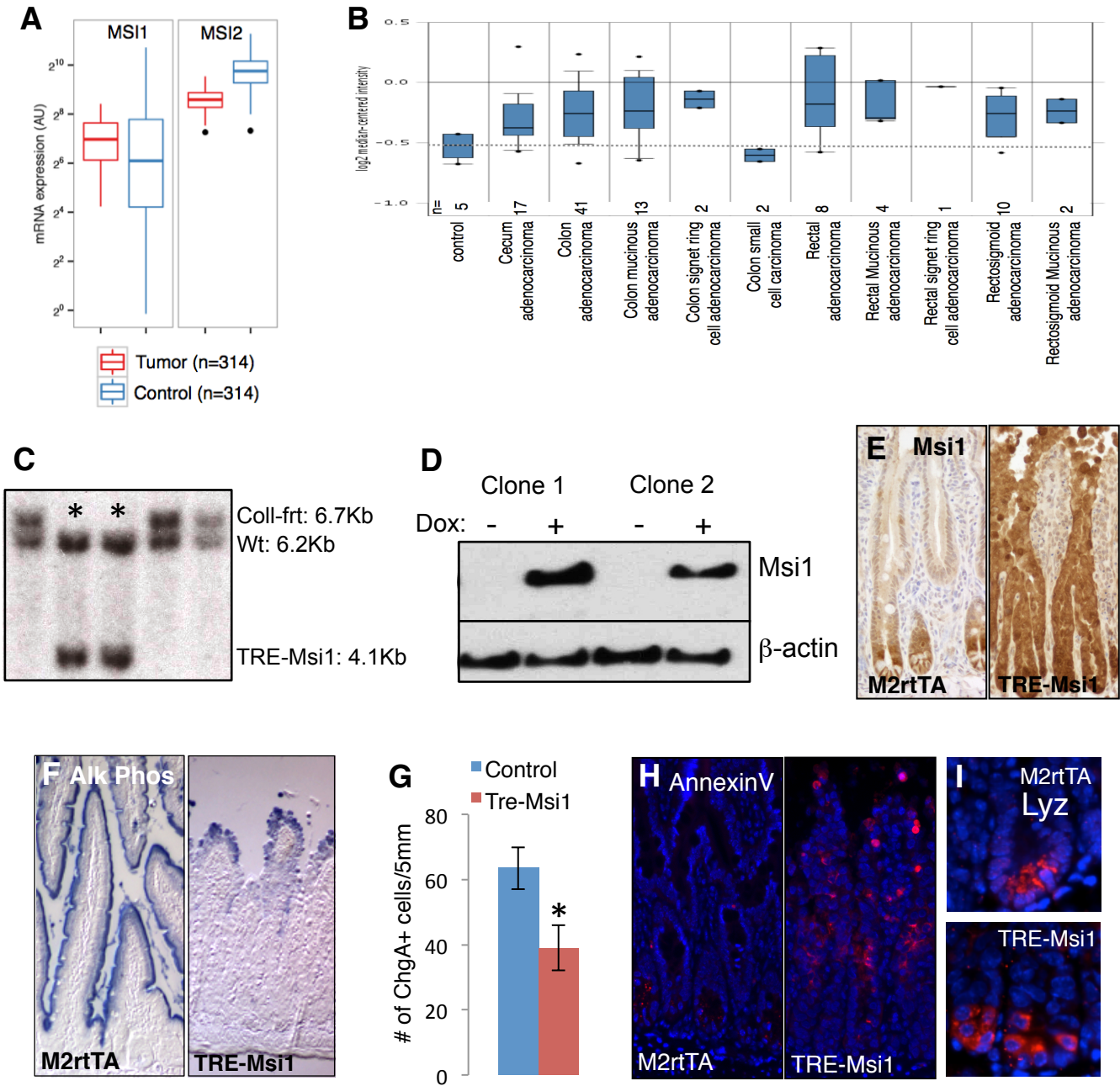
Supplemental Information

## **The Msi Family of RNA-Binding Proteins Function**

### **Redundantly as Intestinal Oncoproteins**

**Ning Li, Maryam Yousefi, Angela Nakauka-Ddamba, Fan Li, Lee Vandivier, Kimberly Parada, Dong-Hun Woo, Shan Wang, Ammar S. Naqvi, Shilpa Rao, John Tobias, Ryan J. Cedeno, Gerard Minuesa, Katz Y, Trevor S. Barlowe, Alexander Valvezan, Sheila Shankar, Raquel P. Deering, Peter S. Klein, Shane T. Jensen, Michael G. Kharas, Brian D. Gregory, Zhengquan Yu, and Christopher J. Lengner**

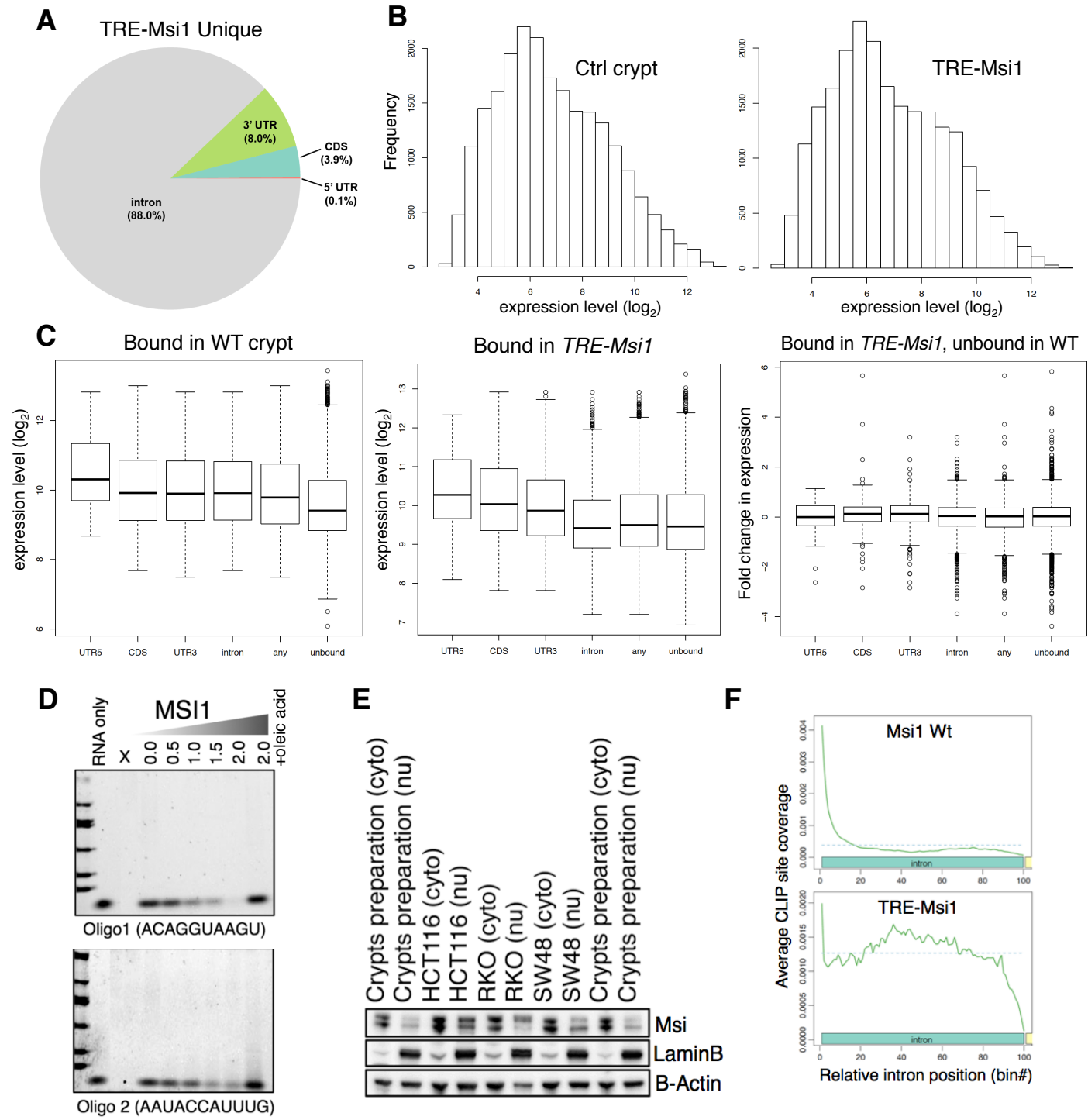
# Supplemental Figure 1



**Supplemental Figure 1, related to Figure 1. A.** TCGA data analysis comparing expression of MSI1 vs. MSI2 in a panel of 314 colorectal adenocarcinomas and 314 normal controls (non patient-matched). **B.** Oncomine transcriptome profiling data of *MSI1* expression in a panel of human gastrointestinal cancers relative to control tissue. The number of samples for each tumor type are indicated. **C.** Southern blot demonstrating correct flip-in targeting (asterisk) of the *TRE-Msi1* allele downstream of the *Coll1a1* locus. **D.** Dox-induction of the *TRE-Msi1* allele in targeted ES cell clones shown by immunoblot. **E.** Immunohistochemistry for Msi1 in control (*M2rtTA*+Dox) and *TRE-Msi1* intestinal epithelium 48hrs after Dox induction. **F.** Staining for Alkaline Phosphatase activity in enterocytes of control (*M2rtTA*+Dox) and *TRE-Msi1* intestinal epithelium. **G.** Quantification of Chromogranin-A-positive enteroendocrine cells per 5mm of small intestine (micrograph shown in Main Figure 1H). \*:  $p < 0.05$ ,  $n = 4$  mice per group. **H.** Immunofluorescence staining for apoptotic cells with annexin-V. **I.** Immunofluorescence detecting Paneth cells at the crypt base via Lysozyme staining in control (*M2rtTA*) and *TRE-Msi1* mice treated with Dox for 48 hours (mag. 400x).

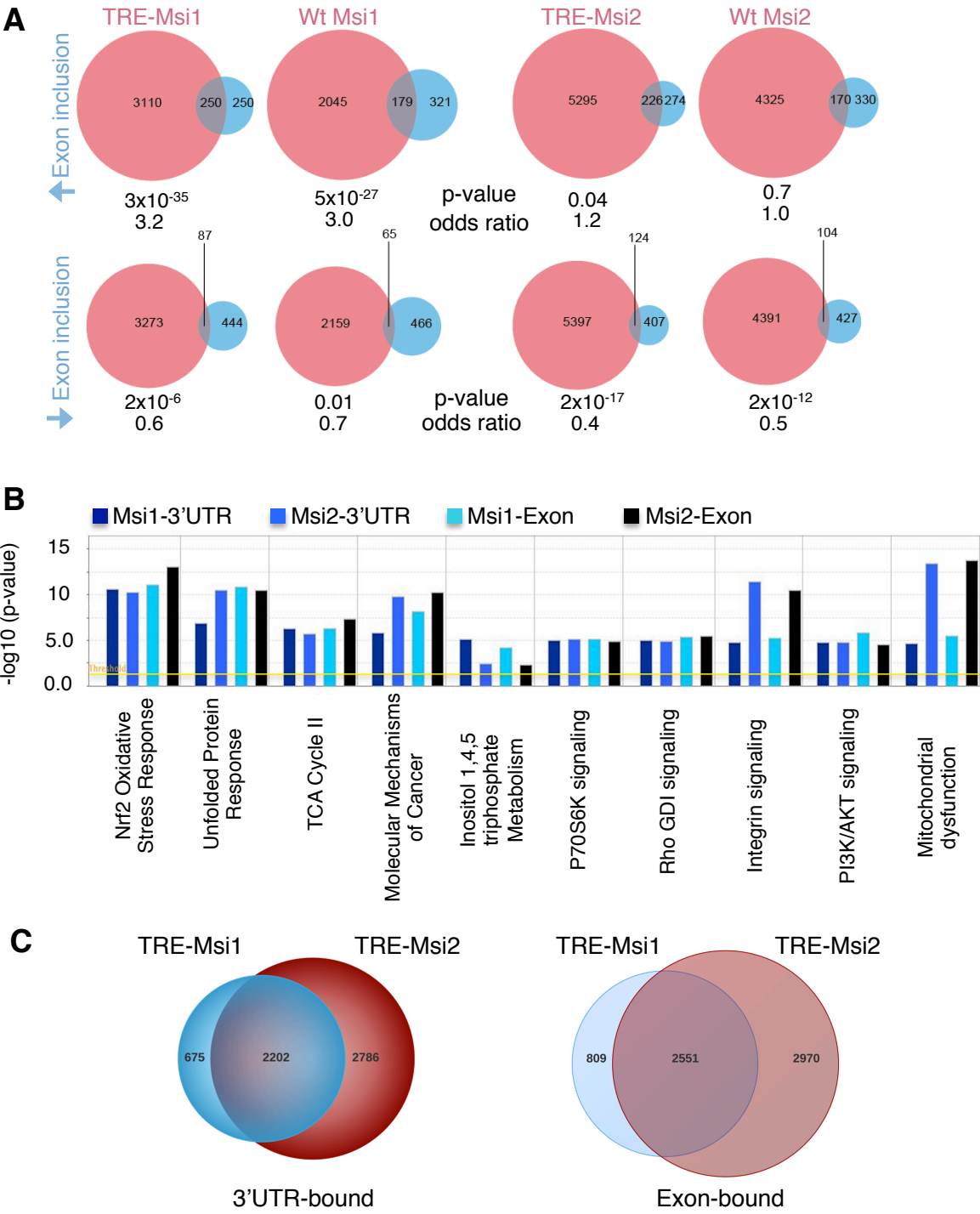


# Supplemental Figure 2



**Supplemental Figure 2, related to Figure 3.** **A** Distribution of Msi1 binding events occurring only in *TRE-Msi1* epithelium and not in wildtype crypts. **B** Expression levels of Msi1 CLIP targets plotted against the frequency of binding events in wildtype crypts and *TRE-Msi1* epithelium. **C** Expression levels of Msi1 CLIP targets of various classes, including the change in expression of genes newly bound after *TRE-Msi1* activation relative to wildtype crypts (right panel). **D** Msi1 RNA binding assays demonstrating dose-dependent interaction between Msi1 and consensus motif oligos derived from CLIP studies (shown in **Figure 3d**). Msi1 binding is competed by the known allosteric Msi inhibitor oleic acid. **E** Cytoplasmic-Nuclear (cyto/nu) fractionation of human colorectal cancer cell lines and primary wildtype intestinal crypts showing predominantly cytoplasmic Msi localization, with detectable nuclear localization particularly in cancer cells. **F** Metaprofiles for Msi1 binding location across introns.

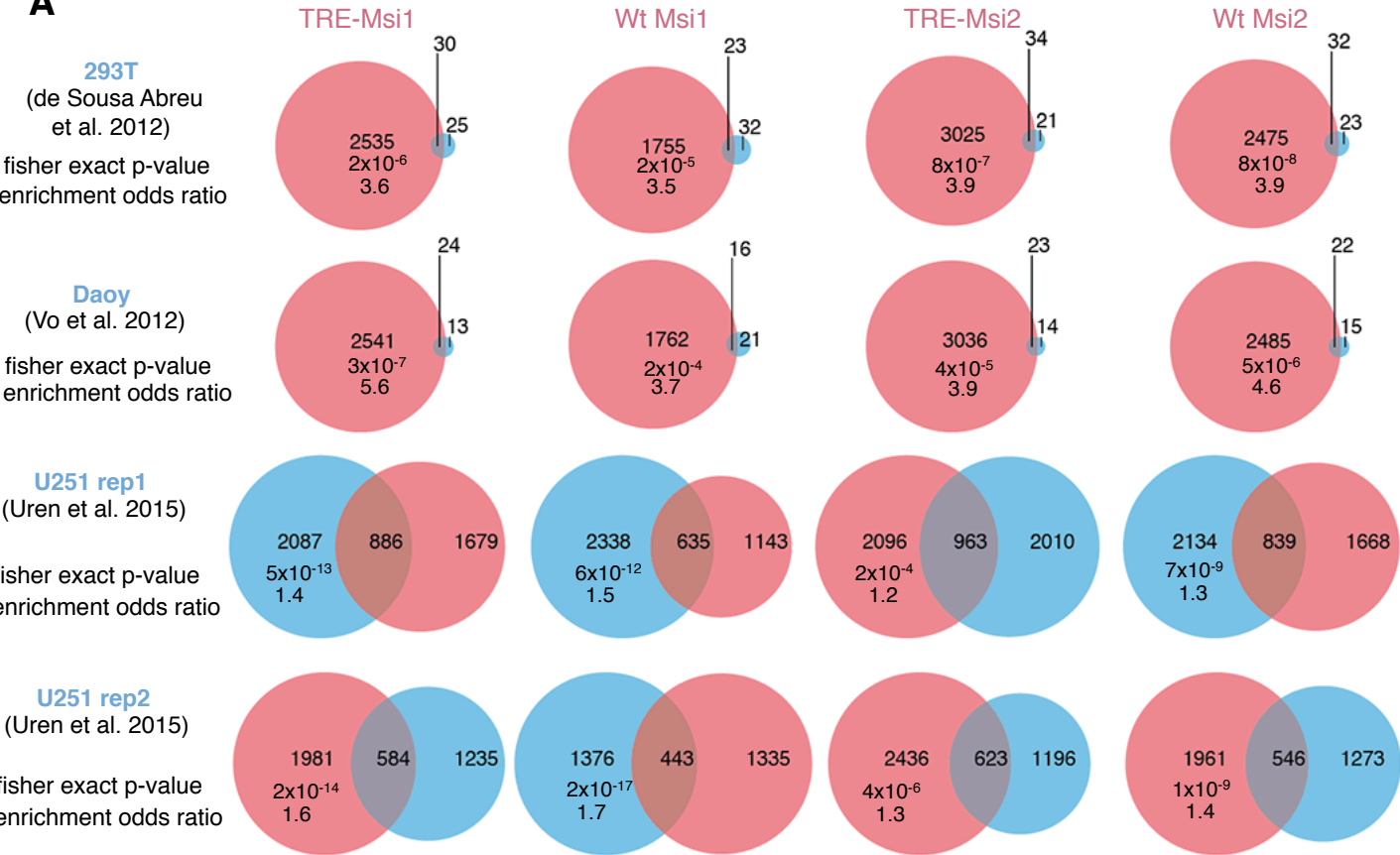
# Supplemental Figure 3



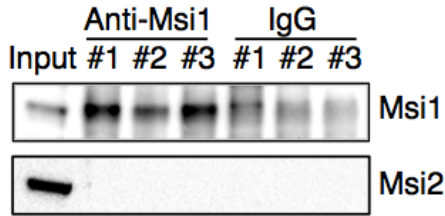
**Supplemental Figure 3, related to Figure 3. A.** Msi CLIP target overlap with transcripts exhibiting alternative splicing in upon Msi1 induction. Transcripts exhibiting increased exon inclusion (blue circles, top) or decreased exon inclusion (blue circles, bottom) in *TRE-Msi1* epithelium vs. control were overlapped with Msi CLIP targets (CLIP target sets indicated in red). **B.** Ingenuity Pathway Analysis (IPA) of canonical pathways represented in Msi CLIP target sets. p-values are derived using Fisher's exact test. **C.** Venn diagrams showing overlap between Msi1 and Msi2 RNA-binding targets in total epithelium from *TRE-Msi1* and *TRE-Msi2* mice.

Supplemental Figure 4

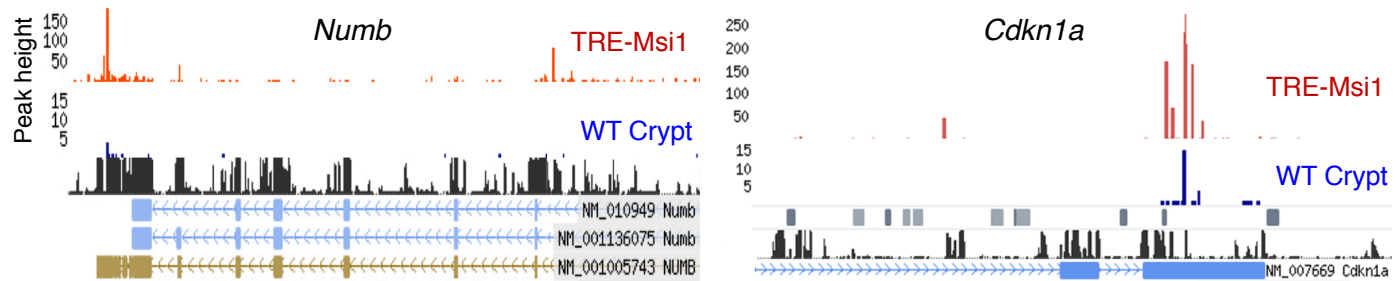
A



B



C

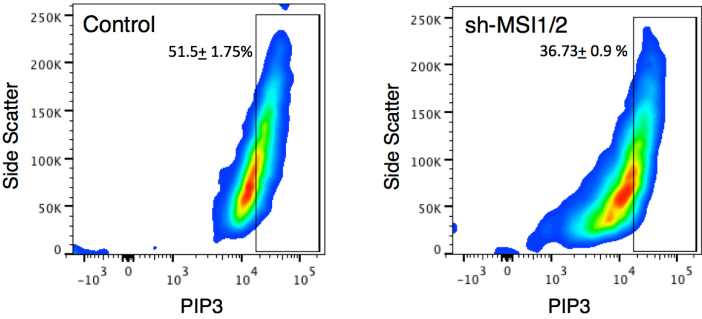


**Supplemental Figure 4, related to Figure 3. A.** Overlap between Msi1 or Msi2 CLIP targets identified in our *in vivo* dataset and MSI1 targets identified *in vitro* in transformed human cell lines (DAOY medulloblastoma, HEK293T embryonic kidney, and two replicates of U251 glioblastoma). **B.** Immunoprecipitation of Msi1 followed by Western blotting for Msi1 and Msi2 revealing no detectable protein-protein interaction **C.** CLIP-Seq tracks showing Msi1 binding to the transcripts encoding Numb (left) and p21 (Cdkn1a, right).

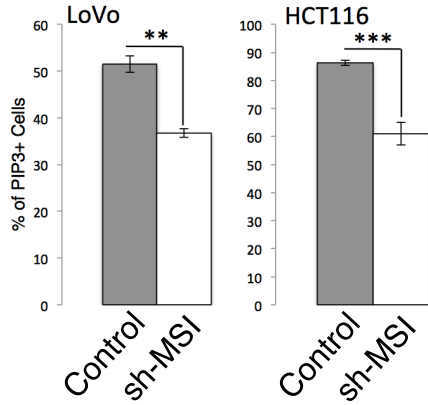


Supplemental Figure 5

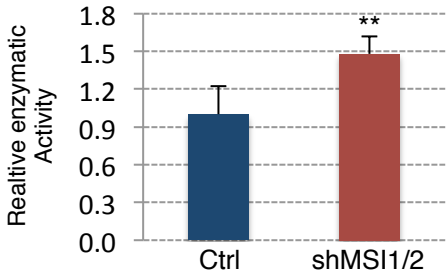
**A**



**B**

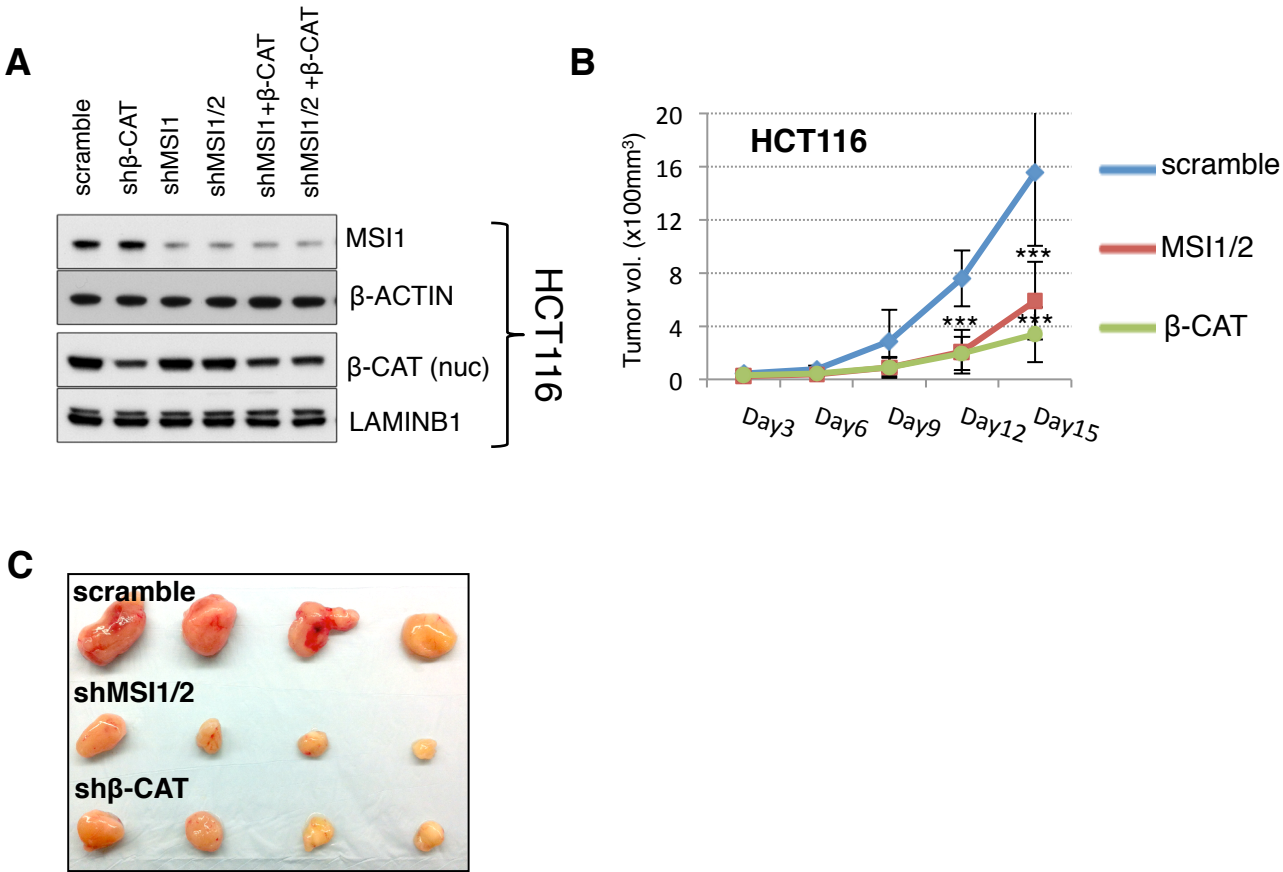


**C**



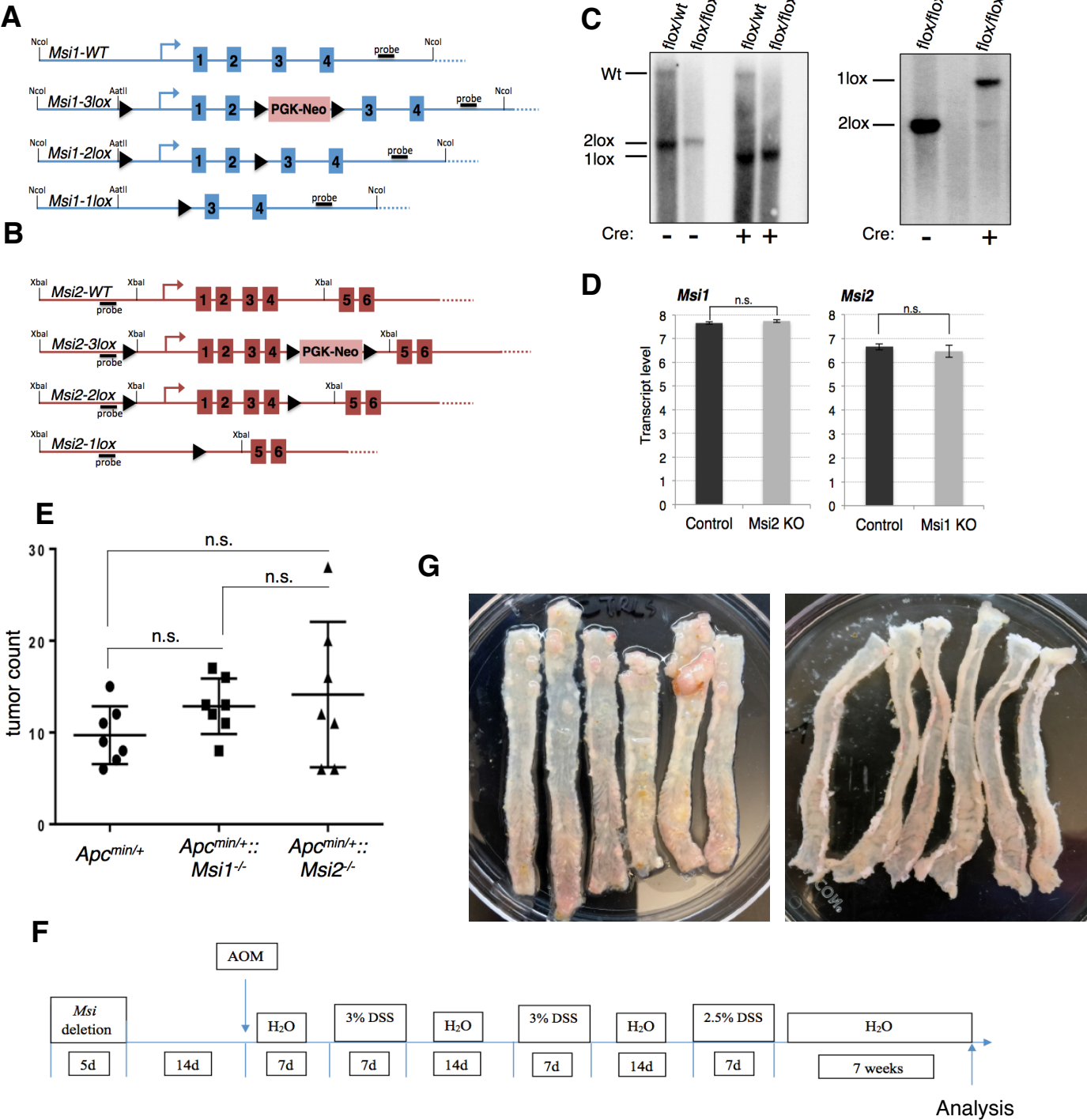
**Supplemental Figure 5, related to Figure 5. A.** Flow cytometric analysis of PIP3 in LoVo cells upon knockdown of MSI1 and MSI2. **B.** Quantification of PIP3 flow cytometric analysis shown in (A) in LoVo and HCT116 cells upon MSI1/2 knockdown. **C.** PTEN enzymatic activity (measured by immunoprecipitation followed by ELISA) increases upon knockdown of MSI1/2 in RKO cells versus scrambled shRNA control. \*\*:  $p < 0.005$ , \*\*\*:  $p < 0.0005$ ,  $n=3$ , Student's t-test.

# Supplemental Figure 6



**Supplemental Figure 6, related to Figure 6. A.** Immunoblotting for MSI1 and nuclear B-CATENIN in HCT116 cells. **B-C.** Growth of HCT116 cell xenografts upon MSI or  $\beta$ -CATENIN shRNA knockdown (**B**), with tumors shown after dissection upon termination of the experiment (**C**). \*\*\*:  $p < 0.0005$ ., Student's t-test.

Supplemental Figure 7



**Supplemental Figure 7, related to Figure 7. A, B.** Targeting strategy showing the 3-lox alleles after homologous recombination in ES cells, the 2-lox (floxed) alleles used to generate mouse strains after transient Cre introduction to excise the PGK-Neo cassette in culture, and the 1-lox, null allele generated after Cre recombinase activity from the Villin-CreER transgene *in vivo*. **C.** Validation of Villin-CreER deletion of Msi1 and Msi2 by Southern blotting after digestion of genomic DNA with XbaI using an external 5' probe depicted in **A, B**. **D.** Expression levels of Msi1 in Msi2KO mice one week after Villin-CreER deletion, and of Msi2 in Msi1KO mice. **E.** Intestinal adenoma counts from APC<sup>min/+</sup> mice, APC<sup>min/+</sup>::Msi1<sup>-/-</sup> mice, and APC<sup>min/+</sup>::Msi2<sup>-/-</sup> mice after deletion of Msi genes using Villin-CreER, n=6-7 mice per group. **F.** Schematic of AOM-DSS protocol. Msi1/2 deletion is mediated by Villin-CreER **G.** Photograph of colons resected from control (left) and Msi1/2 double knockout (right) mice at the end of the AOM-DSS protocol.



## Supplemental Tables

### **Supplemental Table 1, related to Figure 2: TRE-Msi1 transcriptome profiling.**

Expression profiling data for Dox-inducible Msi1 expression in primary small intestinal epithelium 24 hours after Dox induction versus control epithelium.

**Supplemental Table 2, related to Figure 2: Gene Set Enrichment Analyses for TRE-Msi1 transcriptome changes.** GSEA results derived from querying the TRE-Msi1 vs. Control transcriptome profiles from Supplemental Table 1 against the C2 curated all database.

**Supplemental Table 3, related to Figure 3: Gene Ontology Analyses for Msi1 vs. Msi2-induced transcriptome changes.** DAVID GO analysis of transcriptome changes common to both TRE-Msi1 and TRE-Msi2 versus control, as well as those unique to Tre-Msi1 or Tre-Msi2.

**Supplemental Table 4, related to Figure 3: Msi1 RNA binding targets.** *In vivo* RNA binding targets of Msi1 identified by crosslinking, immunoprecipitation, and massively parallel sequencing (CLIP-Seq), including endogenous Msi1 (small intestinal crypts) and ectopic Msi1 24 hours after Dox induction in the intestinal epithelium.

**Supplemental Table 5, related to Figure 3: Gene Ontology Analyses for Msi1 vs. Msi2 *in vivo* RNA binding targets.** GO analysis including endogenous Msi1/2 (small intestinal crypts) and ectopic Msi1/2 24 hours after Dox induction in the intestinal epithelium. Also included is the analogous analysis for an unrelated RNA binding protein, Lin28b.

**Supplemental Table 6, related to Figure 3: Ingenuity Pathway Analysis (IPA) for Msi1/2 RNA binding targets.** IPA analysis for pathways enriched in the Msi1 and Msi2-bound transcript list, bound either in their 3'UTRs or in exonic regions.

## Supplemental Methods

### *Doxycycline Induction and Isolation of Intestinal Epithelium*

For Dox induction of control (*M2rtTA* alone), and *TRE-Msi1* mice, 0.2-2mg/mL of Dox (Doxycycline hyclate, Sigma) was added to the drinking water along with 1% w/v sucrose of mice 2-3 months of age. All analysis of Dox-induced epithelium was performed 48 hours after induction, unless stated otherwise (24 hours used for CLIP and transcriptome profiling). For isolation of intestinal epithelial cells, mouse intestine was cut longitudinally and washed 2-3 times with ice-cold PBS, then cut into small pieces (1 cm long) and incubated for 1 hour at 4 °C in PBS containing 2 mM EDTA and 0.2 mM DTT on a rotating platform. Intestinal epithelial

cells were released by vortexing. For isolation of intestinal crypts, mouse small intestine was isolated and rinsed in PBS as above. The villi were scraped using a hemocytometer coverslip. The crypts were released from murine small intestine by incubation for 30 min at 4 °C in PBS containing 2 mM EDTA. Isolated crypts were counted and pelleted as described in (Sato et al., 2009).

#### *Administration of Rapamycin*

Rapamycin (LC Laboratories) was administered by daily intraperitoneal injection (4 mg per kg of body weight) for 5 days. It was reconstituted in absolute ethanol at 10 mg/ml and diluted in 5% Tween-80 (Sigma) and 5% PEG-400 (Hampton Research) before injection. The final volume of all injections was 200  $\mu$ l. Dox was administered to *TRE-Msi1* mice for 48 hours after the third dose of Rapamycin prior to euthanasia.

#### *Histology, Immunofluorescence, and Immunochemistry*

Intestines were washed with PBS, fixed in 10% Formalin, paraffin-embedded and sectioned. Hematoxylin, eosin, Alcian blue, and Alkaline Phosphatase staining was performed in the Morphology Core of the Penn Center for Molecular Studies in Digestive and Liver Diseases. For immunohistochemistry staining, antigen-retrieval was performed by heating slides in 0.01 M citrate buffer (pH 6) with a pressure cooker. The sections were then immunostained by the ABC peroxidase method (Vector labs) with diaminobenzidine (DAB) as the enzyme substrate and hematoxylin as a counterstain. For detection of nuclear  $\beta$ -catenin, antibody clone 15B8 (Sigma; 1:1000) was used in combination with the MOM kit (Vector Laboratories). For immunofluorescence staining, paraffin sections were pretreated in 0.01 M citrate buffer (pH 6) with a pressure cooker, and incubated in primary antibodies, then incubated with Cy2- or Cy3- conjugated fluorescent secondary antibodies (Jackson Laboratory) and counterstained with DAPI in mounting media (Vector labs). The following antibodies were used: Ki67 (Leica), Msi1 (MBL), Lysozyme (Santa Cruz), Chromogranin A (Abcam), GFP (Abcam). Crypt numbers per 1 mm were counted based on 25 randomly selected areas (Figure 1i). Crypt numbers per 1 mm were counted based on 20 randomly selected areas in proximal and distal intestine (Figure 5F), crypt height was measured based on 40 crypts (Figure 5G) (n=3 independent pairs of mice).

### *CLIP-Seq and CLIP-qRT-PCR*

CLIP-Seq libraries were made as previously described in (Chi et al., 2009) with modifications. Total intestinal epithelial cells from two individual *TRE-Msi1* mice treated with Dox for 24 hours were isolated as above, and wildtype intestinal crypts from two control mice were isolated as above. For crosslinking, cell suspension was exposed to 2 pulses of 265nm UV light at 400mJ/cm<sup>2</sup> in a Stratalinker (Model 2400, Stratagene). Epithelial cells were then lysed using PXL buffer (PBS, 01% SDS, 0.5% deoxycholate, 0.5% NP-40, plus protease inhibitor and RNasin). The lysates were sequentially treated with DNaseI and RNase, and spun in ultra-microcentrifuge at 40,000g for 20 min. The supernatant was added to protein A Dynabeads (Dyna, 100.02) conjugated with Msi1 antibody (AB5977, Millipore) and incubated for 4 hours at 4 °C. <sup>32</sup>P- $\gamma$ -ATP labeled 3' RNA (RL-3) linker was ligated to the RNA fragment on beads overnight at 16°C. The beads were re-suspended in 30  $\mu$ l of Novex loading buffer (without reducing agent), and separated with Novex NuPAGE 10% Bis-Tris gel and transferred to S&S BA-85 nitrocellulose membrane. After overnight exposure, around 50 KD band was visualized and the corresponding membrane was cut to small pieces. The RNA was released by proteinase K digestion and isolated using RNA phenol and CHCl<sub>3</sub> solution. 5' RNA (RL-5) linker was ligated into the RNA fragments. The RNA was transcribed into complementary DNA using RT-PCR and amplified using Re-PCR with Solexa fusion primers. The CLIP library underwent single-end sequencing on an Illumina hiSeq2000 at the University of Pennsylvania Functional Genomics Core. RL-3: 5'-OH GUG UCA GUC ACU UCC AGC GG 3' –puromycin; RL-5: 5' –OH AGG GAG GAC GAU GCG G 3'-OH. Adaptor sequences ('GTGTCAGTCACTTCCAGCG') were removed from the 3' end using the fastx-toolkit ([http://hannonlab.cshl.edu/fastx\\_toolkit/](http://hannonlab.cshl.edu/fastx_toolkit/)). Reads were then mapped using Bowtie (-k 100 -n 0) to the mouse genome (mm9) (Langmead et al., 2009). Peaks were then called using an FDR  $\leq$  0.05 and motifs were identified using Homer (<http://biowhat.ucsd.edu/homer/>). The peaks were then annotated using a set of customized Perl and R scripts. CLIP-Seq datasets are available through GEO, accession number GSE54598.

For CLIP-qRT-PCR, HEK 293 cells treated with GSK3 $\beta$  inhibitor or untreated control were crosslinked and immunoprecipitated with anti-MSI1 antibody as above. Immunoprecipitated



RNA was subjected to quantitative RT-PCR analysis after reverse transcription using a first strand synthesis kit (Invitrogen) and primers specific to the 3'UTRs of *APC* or *CTTNB1* in an ABI Prism quantitative PCR machine using standard 2 stage cycling protocols and SYBR green detection (n=3 biological replicates).

### *Gene Ontology Enrichment*

Gene Ontology enrichment analyses of transcripts with Msi1 and Msi2 binding sites was performed using the DAVID online tool as previously described (Huang da et al., 2009). We define a background set of transcripts accessible to CLIP analysis as those with detectable expression in a tissue-matched RNA-Seq dataset (Middendorp et al., 2014). For this analysis, multiple isoforms of a single gene were only counted as one gene. To reduce bias in reporting GO terms, we report all GO terms within fourteen branches of the “biological process”, “molecular function”, and “cellular component” roots, as determined by a depth first search (Vandivier et al., 2013). Only terms enriched at FDR < 0.05 in at least two samples are reported.

### *Overlap with Published Human Msi1 CLIP and RIP Datasets*

Only transcripts with homologues in both mice and humans were considered in this analysis. Human transcripts with RIP-Seq peaks (de Sousa Abreu et al., 2009; Vo et al., 2012) or CLIP-Seq peaks (Uren et al., 2015) were overlapped with mouse transcripts containing Msi1 and Msi2 CLIP-Seq peaks from our analysis. For significance testing, we define a “universe” of accessible transcripts as all mouse transcripts with 1) homology to human transcripts and 2) detectable expression in a tissue-matched RNA-Seq dataset (Middendorp et al., 2014). Significance of overlap was determined using a Fisher’s Exact test.

### *Overlap with Alternatively Spliced Transcripts*

Exons with significantly (FDR < 0.05) higher or lower inclusion in Msi1 transgenic (TG) over wildtype (WT) were determined by microarray analysis, with three replicates of each genotype. All transcripts represented on the microarray exclusively show increased or decreased exon inclusion and not a combination of the two. Transcripts with differential exon inclusion were then overlapped with transcripts containing Msi1 and Msi2 CLIP-seq peaks in

our analysis. For significance testing, we define a “universe” of accessible genes as those 1) present on the microarray and 2) with detectable expression in a tissue-matched RNA-seq dataset (Middendorp et al., 2014). Significance of overlap was determined using a Fisher’s Exact test.

### *Intron CLIP-Seq Peak Metaprofiles*

CLIP-Seq peak coverage was computed at all mm9 RefSeq introns. Each intron was then length-normalized by binning to 100 intervals, and the average of bins across all introns is plotted as a meta-intron.

### *Transcriptome Profiling*

Total RNA was isolated from total mouse small intestinal epithelial cells from 3 *M2rtTA* and 3 *TRE-Msi1* mice administered Dox for 24 hours in the drinking water using TRIzol Reagent (Life Technologies) according to the manufacturer’s instructions. Total RNA was DNase treated with an RNase-free DNase kit (Zymo Research). Purified RNA was submitted to the University of Pennsylvania Molecular Profiling Core, where samples were labeled and hybridized to Affymetrix Mouse Gene 1.0ST arrays. Microarray data was analyzed using Partek<sup>®</sup> Genomics Suite<sup>™</sup> software. Following RMA background subtraction and normalization, a 1-way-ANOVA analysis between controls (*M2rtTA*) and Msi1 induced (*TRE-Msi1*) was run to compute *p-values* of significance and *F-statistic* for each probeset. *q-value*, a measure of false discovery rate (FDR) was computed within the SAM (Significance Analysis of Microarrays) software for each probeset by running an unpaired *t-test*. The FDR values were integrated with the 1-way-ANOVA results. Genes that were significant at FDR cut-off of 5% and changed at least 2-fold in either direction in the Msi1 induction group when compared to the control group were selected as the set of differentially expressed genes. This set of 836 unique genes and 6 samples were subjected to agglomerative hierarchical clustering analysis. Log2 intensities were median-centered across samples. Euclidean distance was used as the dissimilarity metric and average linkage method as clustering strategy. Results were visualized as intensity heatmap (Figure 2E). GEO accession numbers for microarray datasets are pending. Gene set enrichment analysis (GSEA) was run against the c2 curated gene sets of the Molecular Signatures Database (MSigDB) v3.0 comparing *M2rtTA* and *TRE-*

*Msi1* groups to find statistically significant enriched gene sets.

For analysis of direct  $\beta$ -catenin target gene expression in Figure 4H, genes with published evidence for direct regulation by  $\beta$ -catenin demonstrated by chromatin immunoprecipitation were selected. These genes include *Edn1*, *Fra-1 (Fosl1)*, *c-Myc*, *Met*, *c-Jun*, *Pinx1*, *Tcf4*, *Egfr*, *Klf5*, *Cyclin D (Ccnd1)*, *Mycbp*, *Mmp7*, *Cdkn2a*, *Vegfa*, *SNAI1*, *Fgf18*, *Gja1 (connexin-43)*, *Axin2*, *Claudin1*, *Runx2*, *Lef1*, *Bglap*, *ENPP2*, *Nrcam*, *DLK1*, *Vcan*, *Fgf4*, *Fn1*, *Tcf1*, *(Hnf1a)*, *Lgr5*, *Ppard*, *Sp5*, *Ovol1*, *Id2*, *L1CAM*, *Cdh1 (E-cadherin)*, *Fst*, *Tnfrsf19*, *Neurod1*, *Ctla4*, *Wisp1*, *Fzd7*, *Mitf*, *Pou3f2*, *Gbx2*, *Nkx2-2*, *Neurog1*, *Eda*, *T*, *Pitx2*, *Btrc*, *Cdx1*, *Birc5 (survivin)*, *Pkd1*, *Pml*, and *Lect2 (chemotaxin2)*.

### Reporter Assays

HCT116 cells were plated in 24-well-plate and transfected, in triplicate, with 0.5 $\mu$ g reporter vector (TOPflash Wnt reporter, FOPflash control reporter) together with 0.5 $\mu$ g of the human MSI1 expression vector (in pCDNA6) using FUGENE 6 transfection reagent (Promega). 48h after transfection cells were harvested for reporter assay using the Dual Luciferase Reporter Assay Kit (Promega) according to manufacturer's instruction. Reporter activity was measured using a Fluoroskan Ascent FL (Thermo).

### Western Blots

Cells were lysed in RIPA buffer with protease inhibitors (Roche). After quantification using a BCA protein assay kit (Pierce), 20  $\mu$ g of total protein was separated by 12% SDS-PAGE under denaturing conditions and transferred to PVDF membranes (GE Healthcare). Membranes were blocked in 5% BSA (Sigma) and then incubated with an anti-Msi1 primary antibody (1:1,000; Abcam), NICD (1:1,000; Abcam), Hes1 (1:1,000; Abcam), p-c-Raf (1:1,00; Cell Signaling), p-AKT (T308) (1:1,000; Cell Signaling), p-AKT (S473) (1:1,000; Cell Signaling), total-AKT (1:1,000; Cell Signaling), p-PDK1 (S241) (1:1,000; Cell Signaling), p-4EBP1 (T37/46) (1:1,000; Cell Signaling), or p-eIF4E (S209) (1:1,000; Cell Signaling), followed by incubation with a secondary antibody conjugated with horseradish peroxidase (HRP) (1:2,000; Cell Signaling) together with an HRP-conjugated primary antibody for  $\beta$ -actin

(1:10,000; Sigma). Immunoreactive proteins were visualized using LumiGLO chemiluminescent substrate (Pierce).

### *Oncomine and TCGA*

Using Oncomine analysis, MSI1 expression was analyzed in the Kaiser colon database. The database includes full transcriptome profiles of 105 samples: Control (5); Cecum Adenocarcinoma (17); Colon Adenocarcinoma (41); Colon Mucinous Adenocarcinoma (13); Colon Signet Ring Cell Adenocarcinoma (2); Colon Small Cell Carcinoma (2); Rectal Adenocarcinoma (8); Rectal Mucinous Adenocarcinoma (4); Rectal Signet Ring Cell Adenocarcinoma (1); Rectosigmoid Adenocarcinoma (10); Rectosigmoid Mucinous Adenocarcinoma (2). (Rhodes et al., 2007) For TCGA analysis, fold changes for MSI1 in matched tumor/control RNA-Seq sample pairs from TCGA COAD were calculated (total of 26 patients.) Distribution of MSI1 fold changes in tumor/control pairs for 26 individuals plotted are in red (intra-individual comparison). Distribution of MSI1 fold changes between control/control comparisons for 26 distinct individuals plotted in grey (inter-individual comparison).

### *PTEN Immunoprecipitation and Activity Assay*

Cells (293 & RKO) from a 100 mm culture dish at 70-80% were lysed with 0.5 mL of ice cold IP Lysis Buffer (25mM Tris pH 8.0, 150 mM NaCl, 1% NP-40, 1mM EDTA, 5% Glycerol). 400  $\mu$ L of the cell lysate was Transferred to a fresh, cold, 1.5 mL centrifuge tube. 8  $\mu$ L of the anti-PTEN antibody (Cell Signaling, #9188) was added to the lysate followed by overnight incubation at 4°C with agitation. 60  $\mu$ L of the Protein A Dynabeads was added to the mixture and incubated 2-3 hours at 4°C. The bead complex was washed and resuspended in 30  $\mu$ L of PTEN Reaction buffer. Proceed immediately with the PTEN reactions by adding 30  $\mu$ L of the 16  $\mu$ M PI(3,4,5)P3 Substrate to the bead complex. The ELISA was performed following manufacturer's protocol (Echelon, K-4700).

### *PIP3 Flow Cytometry*

Colorectal cancer cell lines were cultured in DMEM+ 10% FBS and transfected with pSico vector to knockdown Msi1 and Msi2 using Fugene HD (Promega) according to user manual.



EGFP is expressed from pSico as a marker to select for transfected cells. Transfected cells were harvested by trypsinization 72 hours post-transfection, washed and resuspended in PBS containing 1  $\mu$ L/ml of fixable viability dye eFluor 450 (Affymetrix ebioscience). Cells were incubated on ice for 30 minutes and were washed two times with PBS. Then, cells were fixed and permeabilized using Cytofix/ Cytoperm solution (BD PharMingen), stained with FITC-anti-GFP (Abcam) and biotinylated anti-PIP3 (Echelon inc.) for 30 min on ice and washed twice. They were incubated with Streptavidin-Allophycocyanin (APC) (biolegend) for 30 min on ice and washed twice. Flow cytometry was performed on LSRFortessa and Flowjo software was used for data analysis.

### *qRT-PCR*

Human colorectal cancer cell lines were grown to 60-80% confluence followed by RNA extraction with TRIzol. Normal human colon samples were obtained from the Cooperative Human Tissue Network (CHTN) in cooperation with the University of Pennsylvania Center for Molecular Studies in Digestive and Liver Diseases Molecular Biology and Gene Expression Core. RNA from human colon samples and intestinal organoids was isolated with TRIzol.

1  $\mu$ g total RNA was used for reverse transcription in 20  $\mu$ L total volume with High-Capacity cDNA Reverse Transcription Kit (Life Technologies, Cat. No. 4368813). For qRT-PCR, 1  $\mu$ L cDNA product was used for each reaction. Primer sequences used for human MSI1 and MSI2 are as follows: *MSI1#1* Forward: 5'-GCCATGCTGATGTTTCGACAA, Reverse: 5'-CTACGATGTCCTCGCTCTCAA. *MSI1#2* Forward: 5'-AGGACTCAGTTGGCAGACC, Reverse: 5'-GCATCACCAGACACTCTTTCAC. *MSI2#1* Forward: 5'-GCGATGCTGATGTTTCGACAA, Reverse: 5'-TCTCCACAACGTCTTCATTCTCA. *MSI2#2* Forward: 5'-ATTTGCTCCTAGCTATGGCTACC, Reverse: 5'-CGCTGCCACTGGTCCATA

### *Xenograft Assays*

6-week-old female nude mice were obtained from the Stem Cell and Xenograft Core at UPENN. Stably infected colorectal cancer cells were trypsinized and suspended in phosphate-buffered saline (PBS). A total volume of 0.2 ml containing  $2.5 \times 10^6$  cells and 25% volume MatriGEL was injected subcutaneously into the mouse flank. Tumor size was

measured using a Vernier caliper. Tumor volumes were calculated using the formula  $V=1/2(L \times W^2)$ , where L is length (longest dimension) and W is width (shortest dimension) of the tumor. Moribund animals were euthanized according to the protocols of the University of Pennsylvania. Tumor growth rates in the xenograft experiment were evaluated by fitting a linear mixed effects model on the  $\log_{10}$ -transformed tumor volume with days, experiment indicator (Msi shRNA versus control shRNA), and interaction between days and experiment included as independent variables.nat

## Supplemental References

Kinzler, K.W., Nilbert, M.C., Su, L.K., Vogelstein, B., Bryan, T.M., Levy, D.B., Smith, K.J., Preisinger, A.C., Hedge, P., McKechnie, D., *et al.* (1991). Identification of FAP locus genes from chromosome 5q21. *Science* **253**, 661-665.

Levin, T.G., Powell, A.E., Davies, P.S., Silk, A.D., Dismuke, A.D., Anderson, E.C., Swain, J.R., and Wong, M.H. (2010). Characterization of the intestinal cancer stem cell marker CD166 in the human and mouse gastrointestinal tract. *Gastroenterology* **139**, 2072-2082 e2075.

Li, D., Peng, X., Yan, D., Tang, H., Huang, F., Yang, Y., and Peng, Z. (2011). Msi-1 is a predictor of survival and a novel therapeutic target in colon cancer. *Ann Surg Oncol* **18**, 2074-2083.

Li, N., Yousefi, M., Nakauka-Ddamba, A., Jain, R., Tobias, J., Epstein, J.A., Jensen, S.T., and Lengner, C.J. (2014). Single-cell analysis of proxy reporter allele-marked epithelial cells establishes intestinal stem cell hierarchy. *Stem cell reports* **3**, 876-891.

Madison, B.B., Liu, Q., Zhong, X., Hahn, C.M., Lin, N., Emmett, M.J., Stanger, B.Z., Lee, J.S., and Rustgi, A.K. (2013). LIN28B promotes growth and tumorigenesis of the intestinal epithelium via Let-7. *Genes Dev* **27**, 2233-2245.

Marsh, V., Winton, D.J., Williams, G.T., Dubois, N., Trumpp, A., Sansom, O.J., and Clarke, A.R. (2008). Epithelial Pten is dispensable for intestinal homeostasis but suppresses adenoma development and progression after Apc mutation. *Nat Genet* **40**, 1436-1444.

Miyoshi, Y., Nagase, H., Ando, H., Horii, A., Ichii, S., Nakatsuru, S., Aoki, T., Miki, Y., Mori, T., and Nakamura, Y. (1992). Somatic mutations of the APC gene in colorectal tumors: mutation cluster region in the APC gene. *Hum Mol Genet* **1**, 229-233.

Nagase, H., Miyoshi, Y., Horii, A., Aoki, T., Petersen, G.M., Vogelstein, B., Maher, E., Ogawa, M., Maruyama, M., Utsunomiya, J., *et al.* (1992). Screening for germ-line mutations in familial adenomatous polyposis patients: 61 new patients and a summary of 150 unrelated patients. *Hum Mutat* **1**, 467-473.

Naguib, A., Cooke, J.C., Happerfield, L., Kerr, L., Gay, L.J., Luben, R.N., Ball, R.Y., Mitrou, P.N., McTaggart, A., and Arends, M.J. (2011). Alterations in PTEN and PIK3CA in colorectal cancers in the EPIC Norfolk study: associations with clinicopathological and dietary factors. *BMC cancer* **11**, 123.

Nakamura, M., Okano, H., Blendy, J.A., and Montell, C. (1994). Musashi, a neural RNA-binding protein required for *Drosophila* adult external sensory organ development. *Neuron* **13**, 67-81.

Okabe, M., Imai, T., Kurusu, M., Hiromi, Y., and Okano, H. (2001). Translational repression determines a neuronal potential in *Drosophila* asymmetric cell division. *Nature* **411**, 94-98.

Okano, H., Imai, T., and Okabe, M. (2002). Musashi: a translational regulator of cell fate. *J Cell Sci* **115**, 1355-1359.

Park, S.M., Deering, R.P., Lu, Y., Tivnan, P., Lianoglou, S., Al-Shahrour, F., Ebert, B.L., Hacohen, N., Leslie, C., Daley, G.Q., *et al.* (2014). Musashi-2 controls cell fate, lineage bias, and TGF-beta signaling in HSCs. *The Journal of experimental medicine* **211**, 71-87.

Park, S.M., Gonen, M., Vu, L., Minuesa, G., Tivnan, P., Barlowe, T.S., Taggart, J., Lu, Y., Deering, R.P., Hacohen, N., *et al.* (2015). Musashi2 sustains the mixed-lineage leukemia-driven stem cell regulatory program. *The Journal of clinical investigation* **125**, 1286-1298.

Potten, C.S., Booth, C., Tudor, G.L., Booth, D., Brady, G., Hurley, P., Ashton, G., Clarke, R., Sakakibara, S., and Okano, H. (2003). Identification of a putative intestinal stem cell and early lineage marker; musashi-1. *Differentiation* **71**, 28-41.

Powell, A.E., Wang, Y., Li, Y., Poulin, E.J., Means, A.L., Washington, M.K., Higginbotham, J.N., Juchheim, A., Prasad, N., Levy, S.E., *et al.* (2012). The pan-ErbB negative regulator Lrig1 is an intestinal stem cell marker that functions as a tumor suppressor. *Cell* **149**, 146-158.

Rezza, A., Skah, S., Roche, C., Nadjar, J., Samarut, J., and Plateroti, M. (2010). The overexpression of the putative gut stem cell marker Musashi-1 induces tumorigenesis through Wnt and Notch activation. *J Cell Sci* **123**, 3256-3265.

Sakakibara, S., Nakamura, Y., Yoshida, T., Shibata, S., Koike, M., Takano, H., Ueda, S., Uchiyama, Y., Noda, T., and Okano, H. (2002). RNA-binding protein Musashi family: roles for CNS stem cells and a subpopulation of ependymal cells revealed by targeted disruption and antisense ablation. *Proceedings of the National Academy of Sciences of the United States of America* **99**, 15194-15199.

Sanchez-Diaz, P.C., Burton, T.L., Burns, S.C., Hung, J.Y., and Penalva, L.O. (2008). Musashi1 modulates cell proliferation genes in the medulloblastoma cell line Daoy. *BMC cancer* **8**, 280.



Sansom, O.J., Reed, K.R., Hayes, A.J., Ireland, H., Brinkmann, H., Newton, I.P., Batlle, E., Simon-Assmann, P., Clevers, H., Nathke, I.S., *et al.* (2004). Loss of Apc in vivo immediately perturbs Wnt signaling, differentiation, and migration. *Genes Dev* **18**, 1385-1390.

Spears, E., and Neufeld, K.L. (2011). Novel double-negative feedback loop between adenomatous polyposis coli and Musashi1 in colon epithelia. *The Journal of biological chemistry* **286**, 4946-4950.

Subramanian, A., Tamayo, P., Mootha, V.K., Mukherjee, S., Ebert, B.L., Gillette, M.A., Paulovich, A., Pomeroy, S.L., Golub, T.R., Lander, E.S., *et al.* (2005). Gene set enrichment analysis: a knowledge-based approach for interpreting genome-wide expression profiles. *Proceedings of the National Academy of Sciences of the United States of America* **102**, 15545-15550.

Sugiyama-Nakagiri, Y., Akiyama, M., Shibata, S., Okano, H., and Shimizu, H. (2006). Expression of RNA-binding protein Musashi in hair follicle development and hair cycle progression. *The American journal of pathology* **168**, 80-92.

Sureban, S.M., May, R., George, R.J., Dieckgraefe, B.K., McLeod, H.L., Ramalingam, S., Bishnupuri, K.S., Natarajan, G., Anant, S., and Houchen, C.W. (2008). Knockdown of RNA binding protein musashi-1 leads to tumor regression in vivo. *Gastroenterology* **134**, 1448-1458.

Sutherland, J.M., Fraser, B.A., Sobinoff, A.P., Pye, V.J., Davidson, T.L., Siddall, N.A., Koopman, P., Hime, G.R., and McLaughlin, E.A. (2014). Developmental expression of Musashi-1 and Musashi-2 RNA-binding proteins during spermatogenesis: analysis of the deleterious effects of dysregulated expression. *Biology of reproduction* **90**, 92.

Uren, P.J., Vo, D.T., de Araujo, P.R., Potschke, R., Burns, S.C., Bahrami-Samani, E., Qiao, M., de Sousa Abreu, R., Nakaya, H.I., Correa, B.R., *et al.* (2015). RNA-Binding Protein Musashi1 Is a Central Regulator of Adhesion Pathways in Glioblastoma. *Molecular and cellular biology* **35**, 2965-2978.

van Hogezaand, R.A., Eichhorn, R.F., Choudry, A., Veenendaal, R.A., and Lamers, C.B. (2002). Malignancies in inflammatory bowel disease: fact or fiction? *Scandinavian journal of gastroenterology Supplement*, 48-53.

Vo, D.T., Subramaniam, D., Remke, M., Burton, T.L., Uren, P.J., Gelfond, J.A., de Sousa Abreu, R., Burns, S.C., Qiao, M., Suresh, U., *et al.* (2012). The RNA-binding protein Musashi1 affects medulloblastoma growth via a network of cancer-related genes and is an indicator of poor prognosis. *The American journal of pathology* **181**, 1762-1772.

Wang, S., Li, N., Yousefi, M., Nakauka-Ddamba, A., Li, F., Parada, K., Rao, S., Minuesa, G., Katz, Y., Gregory, B.D., *et al.* (2015). Transformation of the intestinal epithelium by the MSI2 RNA-binding protein. *Nature communications* 6, 6517.

Wang, X.Y., Yin, Y., Yuan, H., Sakamaki, T., Okano, H., and Glazer, R.I. (2008). Musashi1 modulates mammary progenitor cell expansion through proliferin-mediated activation of the Wnt and Notch pathways. *Molecular and cellular biology* 28, 3589-3599.

Wasan, H.S., Park, H.S., Liu, K.C., Mandir, N.K., Winnett, A., Sasieni, P., Bodmer, W.F., Goodlad, R.A., and Wright, N.A. (1998). APC in the regulation of intestinal crypt fission. *J Pathol* 185, 246-255.